Predictions of Aneurysm Formation in Distensible Tubes
Part A – Theoretical Background to Alternative Approaches

Andrea Bucchi* (a) and Grant E. Hearn (b)

(a) School of Engineering, University of Portsmouth, United Kingdom

(b) Fluid Structure Interaction Research Group – Faculty of Engineering and the Environment, University of Southampton, United Kingdom

Abstract

Pressurized distensible tubes are subject to aneurysms. Aneurysm inception will take place at a location along the tube when a critical pressure, relative to tube wall thickness at that location, is reached. Parents will recognise the existence of critical pressure when endeavouring to inflate a party balloon. Another example of aneurysm is the thoracic aortic aneurysm corresponding to permanent dilation of the aorta in such proportions that it can be life threatening. Corrective procedures for aortic aneurysms involve the introduction of stiff materials to prevent aneurysm. Similarly in a proposed distensible tube based wave energy device aneurysm inception is partially controlled through the use of alternative longitudinal strips of inextensible material and appropriate rubber strips. Here we consider distensible tubes made of one material.

Having reviewed the aneurysm based literature some inconsistencies were observed between the material properties used in a non-linear finite element analysis and the material properties of the specimen used to provide experimental measurements for comparison. To appreciate the inconsistencies the authors decided to investigate aneurysm development using both non-linear finite element analyses and distinct alternative formulations and solution techniques. Rather than restrict strain-energy function to a subset of Neo-Hookean, Mooney-Rivlin and Ogden forms, the authors have implemented several alternative strain-energy models in parallel, also exploring for the first time the impact of using different combinations of uniaxial, equi-biaxial and pure shear experimental data for different rubbers.

This paper addresses the needs (necessary considerations, such as the Valanis-Landel hypothesis, Maxwell equal area rule and data selection criteria) for a realistic approach to modelling a distensible tube to provide predictions of critical pressure. In common with all other cited references a static analysis is used.

* Corresponding author, e-mail address: Andrea.Bucchi@port.ac.uk

1. Introduction

Within the literature critical pressure is determined from static analysis with differing governing equations solved using alternative techniques. In the finite element approach strain-energy functions are utilised once the appropriate parameters have been determined from experimentally observed material behaviour. Of particular interest in this paper are the challenges and implications of using different experimental data sets and alternative strain-energy functions to determine the value of critical pressure. This is a problem shared in such diverse fields as bio-engineering, fluid-dynamics, mechanical and medical sciences.

The extent of research completed is too large for a single publication. Hence this paper presents the associated theory, with an indication of the derivation of the governing equations (omitted in all related papers found) and provides limited indicative qualitative comparative results. The companion paper presents direct numerical comparisons of predicted results for all different possible data set combinations and several alternative strain-energy functions. Predictions of the selected finite element package used by the authors are compared with an independently published generated finite element analysis.

This paper addresses the identification of a realistic approach to modelling a distensible tube to provide meaningful predictions of critical pressure. In common with all other cited references a static analysis is used.

Appreciation of balloon inflation is addressed by Osborne & Sutherland [1] and Müller & Struchtrup [2]. The investigation of aortic aneurysm is dealt with, in greater detail, by Vorp [3]. Medical investigation of ruptured and intact aortic specimens indicates large diameter increases [4]. More complex tube construction using two distinct materials can lead to critical pressures beyond normal utilisation or occurrence. Medically this corresponds to the introduction of stents for reinforcement of arteries [5]. In engineering, the analysis of the more complex tube constructions used in wave energy devices ensures practical initial set up operational pressures consistent with wave environment. Whilst rubber is seen as a relatively low cost and low maintenance material it can experience different kinds of instability [6, 7]. These examples, taken from different fields of interest, are sufficient to demonstrate the need to predict the likelihood and the prevention of an aneurysm. An appreciation of existing aneurysm research is summarised next.

1.1 Brief review of aneurysm research

Mallock [8] is credited with presenting the first paper addressing the formation of an aneurysm in a pressurised rubber tube. Mallock describes the birth of an aneurysm as 'one or more bulbous expansions' associated with the attainment of a critical radius and hence critical pressure. Alexander [9] and Needleman [10] both investigated such instability during the inflation of spherical shaped rubber balloons. Haughton [11] has addressed perfect and imperfect spherical rubber membranes. Alexander [12] extended the instability studies to cylindrical membranes; Kyriakides & Chang [13, 14] have provided theoretical and experimental comparison of the formation of aneurysms in cylindrical rubber tubes. Kyriakides & Chang observed experimentally that tube radius expanded uniformly along the tube length with increased pressure until critical pressure was attained. Thereafter radial growth was localized at the point of aneurysm initiation. As more fluid is injected into the tube the pressure is reduced and the aneurysm spreads longitudinally until the whole tube approximates a cylindrical shape. Further injection of fluid leads to increased pressure and radial growth until material failure occurs. The axial position of the aneurysm is influenced by manufacturing imperfections (non uniform wall thickness) or geometrical imperfections (radius variations along the tube) or even non homogeneous material properties.

According to Kyriakides & Chang [13, 14] and Kanner & Horgan [15] critical pressure is the peak pressure in the pressure-volume curve. However, Fu et al. [16], indicate that the 'initiation pressure' associated with the initial bulge in the tube occurs within a small (mathematically perceived) neighbourhood of the critical pressure. It is defined as the pressure at which bifurcation occurs. This more precise definition befits theoretical bifurcation investigations (discussed briefly in Section 3.3.2) rather than experimental and engineering studies of aneurysm.

Kyriakides & Chang [14] solved stated governing equations using finite differences subject to fixed and rolled tube end condition. The slightly more detailed formulation of Guo [17] addresses a membrane of general axisymmetric shape. A simpler Guo [18] formulation restricts the initial shape of the membrane to be a uniform circular cylinder. Solutions [17, 18] are generated using a 'shooting' technique (Section 14.1 of [19]) with both tube ends fixed. Yang & Feng [20] formally describe the 'shooting' technique as the application of the Cauchy-Kawalewski theorem when solving ordinary differential equations. That is, a two-point boundary value problem is treated as an initial value problem. The finite element approach can address both situations and with an appropriate choice of elements permits greater flexibility in tube end conditions and removal of

assumed uniform material properties. Shi & Moita [21] developed an axisymmetric hyper–elastic membrane and solved the non-linear static problem with the arc–length method [22]. Pamplona et al. [23] and Goncalves et al. [24] used the Riks algorithm with the ABAQUS® finite element software.

1.2 Comparison of numerical predictions and experimental measurements

Kyriakides & Chang [13, 14] provide very comparable predictions and measurement of critical and propagation pressures, radial stretch ratio values at particular longitudinal positions and pressure variation with radial stretch ratio. Pamplona et al. [23] and Goncalves et al. [24] also report very good agreement between theoretical predictions and experimental measurements. However, closer analysis of [23, 24] and the related PhD dissertation [25] (in Portuguese) suggest that material properties used in the predictions are quite distinct to those of the experimental study. Furthermore, the material stress-strain data is determined from a variant of the standard uniaxial tension test [26]. This limited data base and the apparent degree of agreement between prediction and measurement aroused our interest. In particular, Figure 3 of [24] is generated using the strain-energy function parameters of Table 2 [24]. The close agreement of Neo-Hookean and Mooney-Rivlin fitted strain-energy functions with the experimental data is quite acceptable. However, the first-order Ogden model is quite distinct irrespective of adoption of Equations (15) or (16) of this paper. Furthermore, Table 2 [24] is different to Table 4.4 [25], although the corresponding force versus strain figures in [24] and [25] are identical. These different inconsistently attributed material properties provided the motivation to investigate the role of different selected material models upon critical pressure prediction in aneurysm formation.

1.3 Organization of paper

Fundamental theoretical concepts and definitions regarding continuum mechanics for a hyper-elastic material are presented in Section 2.1. The principal steps to determine strain-energy function parameters from experimental data are presented with definitions of commonly used strain-energy functions attributed to Mooney-Rivlin, Ogden, Treloar (Neo-Hookean), Yeoh, Arruda-Boyce and Marlow in Section 2.2. Section 3 reviews static formulations of differing mathematical complexity for modelling and predicting aneurysm characteristics. Section 3.1 addresses a long cylindrical thin-walled tube, uniformly inflated, whereas a more complex analytic method for an axisymmetric membrane is treated in Section 3.2. The derivation of these two alternative semi-analytical methods

are presented, together with summary algorithms, since the different predictions are studied to appreciate both the appropriateness of the finite element based modelling and to provide a general comparison; a task not previously reported in the literature. The authors' governing equations derivation within Section 3.2 is considered necessary given derivations have not been located in the extensive literature search undertaken. Hence they may be deemed useful to other researchers. The more general finite element method is summarised in Section 3.3 with justification of specific possible choices made regarding its application. Sample representative results for each technique are presented and discussed in Section 4. Finally closure concerning the different mathematical approaches is reported in Section 5. The original Treloar rubber data used [27] has been retrieved as explained in Appendix A. This data, rather than the Ogden fitted [28, 29] Treloar rubber data, used by several authors [10, 21, 30], is utilized in our applications. A second set of tabulated data is due to Kawabata et al. [31]. The sensitivity of fitting different rubber models to different combinations of measured stress-strain data is a novel and extensive in-depth aspect of this research.

2. Mathematical formulation

Following basic definitions of continuum mechanics related variables, this section reviews basic relationship between alternative experimental stress-strain data sets and strain-energy functions. The characteristics of the Treloar and Kawabata et al. data sets and the identification of the strain-energy function parameters using different combinations of the experimental data is summarised prior to defining the strain-energy functions applied.

2.1. Continuum mechanics description of rubber material

A practical definition of a rubber-like material, referred to as a hyper-elastic or Green-elastic material, is a perfect elastic material for which strain-energy function (W) existence can be postulated [28]. A rigorous mathematical definition of a hyper-elastic material is found in [32]. This approach requires the existence of a scalar elastic potential (strain-energy) function, whose derivative with respect to a strain component determines the corresponding stress component as outlined in Section 2.2. Different expressions for the strain-energy function permit development of different constitutive models for a rubber-like material. In general a strain-energy function depends on the stretch tensor $\mathbf{U}$, written as $W = W(\mathbf{U})$. Figure 1 indicates a stretching $\mathbf{U}$ and a rotation $\mathbf{R}$ of a material element. In general the deformation gradient tensor $\mathbf{F}$ associated with stretching followed by rotation can be decomposed as $\mathbf{F} = \mathbf{RU}$. The right Cauchy-Green deformation tensor

$\mathbf{C}$ is defined as $\mathbf{C} = \mathbf{F}^{\mathrm{T}}\mathbf{F}$. For an isotropic material rotation has no influence on material properties and hence W is independent of the stretching orientation [33]. Hence W is expressed as either $W = W(\lambda_1, \lambda_2, \lambda_3)$, a function of principal stretches, $\lambda_i : i = 1, 2 \,\&\, 3$ or as $W = W(I_1, I_2, I_3)$ a function of strain invariants $I_i : i = 1, 2 \,\&\, 3$. (1)

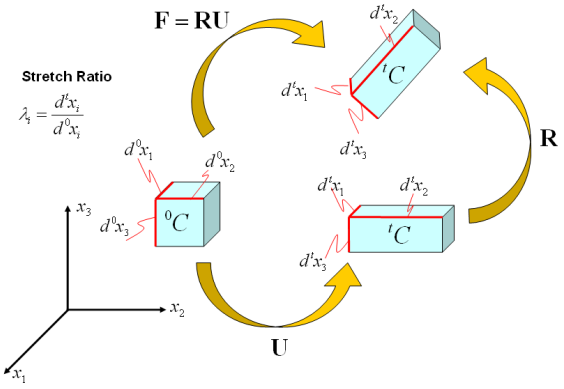

Fig. 1. Basic concepts of continuum mechanics.

For an isotropic material the square of the *principal stretches* (λ_i^2) are the eigenvalues of the right Cauchy-Green deformation tensor $\mathbf{C}$. They are related to *strain invariants* (I_i), in accordance with:

$$I_1 = \lambda_1^2 + \lambda_2^2 + \lambda_3^2, \qquad I_2 = 1/\lambda_1^2 + 1/\lambda_2^2 + 1/\lambda_3^2 \qquad \text{and} \qquad I_3 = \lambda_1^2\lambda_2^2\lambda_3^2. \tag{2}$$

The third invariant $[I_3]$ describes the volume change during the deformation, that is $dv^t = Jdv^0$, see [34]. Hence, for an incompressible material it follows that $J^2 = [\det \mathbf{F}]^2$ i.e. $J^2 \equiv \|diag(\lambda_1 \quad \lambda_2 \quad \lambda_3)\|^2 = I_3$ and thus $I_3 = 1$. Consequently for an isotropic and incompressible material the strain–energy function is simply $W = W(\lambda_1, \lambda_2)$ or $W = W(I_1, I_2)$. The Ogden [28] and Mooney–Rivlin [35] strain-energy functions are dependent on both strain invariants, whereas the Neo–Hookean [27], Yeoh [36], Arruda–Boyce [37] and Marlow [38] strain-energy functions are only dependent upon I_1. More detailed information can be retrieved from original referred papers; brief descriptions are provided in Sections 2.2.2 & 2.2.3.

2.2 Relationship between experimental test and strain-energy function

The strain-energy functions presented in this section have different numbers of parameters. These parameters must be determined from an experimental data set covering the anticipated range of strain to be investigated. In general the experimental data is obtained through a simple uniaxial tension test using a dumbbell shaped test piece. Less common measurement procedures are the pure

shear test, using a long narrow strip of material, and the equi-biaxial tension test in which a sheet of rubber is deployed. Sole use of pure tension testing is extremely hazardous [39]. It is recommended that experimental data is acquired by different deformation modes (tests) [33, 40].

Prior to consideration of parameter identification of the strain-energy function it is necessary to appreciate the relationship between the Cauchy stresses $\sigma_i : i = 1,2 \,\&\, 3,$ for the three possible experimental test procedures. For an isotropic incompressible material the principal Cauchy stresses are defined [29] as:

$$\sigma_i = \lambda_i \frac{\partial W}{\partial \lambda_i} - p \;\; : i = 1,\, 2 \,\&\, 3 \tag{3}$$

where p is an arbitrary hydrostatic pressure consistent with the incompressibility constraint.

Uniaxial tension test:

In this case the principal stretch ratios satisfy: $\lambda_1 = \lambda$ and $\lambda_2 = \lambda_3$. The incompressibility constraint therefore implies that $\lambda_2 = \lambda_3 = 1/\sqrt{\lambda_1} = 1/\sqrt{\lambda}$. (4a)

Given the material is isotropic the principal Cauchy stresses are $\sigma_1 = \sigma$ with $\sigma_2 = \sigma_3 = 0$. Since $\sigma_2 = 0$, the hydrostatic pressure can be eliminated from the expression for σ_1 that is:

$$\sigma_1 = \lambda_1 \frac{\partial W}{\partial \lambda_1} - \lambda_2 \frac{\partial W}{\partial \lambda_2}. \tag{4b}$$

When the strain-energy is expressed in terms of the invariants, $W = W(I_1, I_2)$, Equation (4b) assumes the general form:

$$\sigma_1 = \lambda_1 \left[\frac{\partial W}{\partial I_1}\frac{\partial I_1}{\partial \lambda_1} + \frac{\partial W}{\partial I_2}\frac{\partial I_2}{\partial \lambda_1} \right] - \lambda_2 \left[\frac{\partial W}{\partial I_1}\frac{\partial I_1}{\partial \lambda_2} + \frac{\partial W}{\partial I_2}\frac{\partial I_2}{\partial \lambda_2} \right]. \tag{5}$$

From Equation (2) we note that $\frac{\partial I_1}{\partial \lambda_1} = 2\lambda$, $\frac{\partial I_2}{\partial \lambda_1} = -2\lambda^{-3}$, $\frac{\partial I_1}{\partial \lambda_2} = 2/\sqrt{\lambda}$ and $\frac{\partial I_2}{\partial \lambda_2} = -2\lambda\sqrt{\lambda}$, (6)

and hence, the uniaxial Cauchy stress is:

$$\sigma_1 = 2\lambda\left(1 - \frac{1}{\lambda^3}\right)\left(\lambda \frac{\partial W}{\partial I_1} + \frac{\partial W}{\partial I_2}\right). \tag{7}$$

Whereas the Cauchy stresses are by definition related to the deformed cross-sectional area, the experimental data is often recorded in terms of engineering or nominal stresses t_i referred to the un-deformed cross-sectional area. Since the deformed and the original volume of the material is the same, the ratio of the deformed and original cross-section areas is λ. Hence the Cauchy and nominal stresses are related by: $t_i = \sigma_i / \lambda_i$. Thus the uniaxial nominal stress t_1 is expressed as:

$$t_1 = 2\left(1-\frac{1}{\lambda^3}\right)\left(\lambda\frac{\partial W}{\partial I_1}+\frac{\partial W}{\partial I_2}\right). \tag{8}$$

The formulae for the equi-biaxial and pure shear principal stress can be recovered similarly. Final relationships are therefore stated having indicated derivation process for the uniaxial case.

Equi-biaxial tension test:

In an equi-biaxial tension test the principal stretch ratios satisfy:

$$\lambda_1 = \lambda_2 = \lambda \text{ and so } \lambda_3 = 1/\lambda^2 . \tag{9a}$$

The principal Cauchy stresses are $\sigma_1 = \sigma_2 = \sigma$ with $\sigma_3 = 0$. Consequently the equi-biaxial nominal stress satisfies:

$$t_1 = t_2 = 2\left(\lambda-\frac{1}{\lambda^5}\right)\left(\frac{\partial W}{\partial I_1}+\lambda^2\frac{\partial W}{\partial I_2}\right). \tag{9b}$$

Pure shear test:

For a pure shear test deformation we impose:

$$\lambda_3 = 1,\ \lambda_1 = \lambda \text{ and so } \lambda_2 = 1/\lambda, \tag{10a}$$

with $\sigma_1 = \sigma$ and $\sigma_2 = 0$. The stress σ_3 is non-zero to maintain $\lambda_3 = 1$. It may be readily shown that the nominal planar stress is:

$$t_1 = 2\left(\lambda-\frac{1}{\lambda^3}\right)\left(\frac{\partial W}{\partial I_1}+\frac{\partial W}{\partial I_2}\right). \tag{10b}$$

Equations (8) to (10) provide nominal stresses definition for each experimental test condition.

In non-linear finite element analysis [41], the 2nd Piola-Kirchhoff stress tensor, S_{ij}, is often preferred. In this case the principal stresses are defined as:

$$S_i = \frac{1}{\lambda_i^2}\sigma_i \equiv \frac{1}{\lambda_i}t_i . \tag{11}$$

Identification of σ_i or t_i requires selection of an appropriate strain-energy function W and the fitting of free parameters associated with W using suitable experimental data sets. This is addressed next.

2.2.1 Fitting of strain-energy parameters to selected data sets

Two well known and utilized experimental data sets for rubber are those of Treloar [27] and Kawabata et al. [31]. The characteristics of the rubbers investigated may respectively be described as 8% sulphur vulcanized rubber and isoprene vulcanized rubber. Table 1 provides ranges of

investigated λ-values for uniaxial, equi-biaxial and pure shear tests for both data sets. Plots of engineering stress versus strain for each measurement procedure are presented in Figures 2 & 3 for the Treloar and Kawabata et al. data.

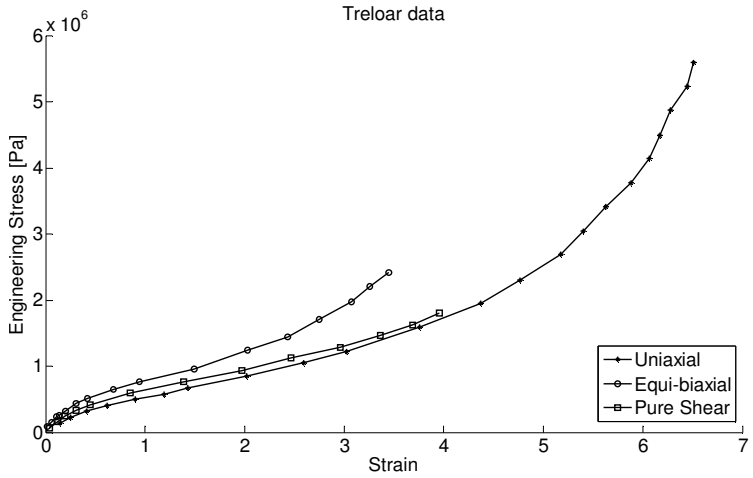

Fig. 2. Treloar data [27] & Appendix A

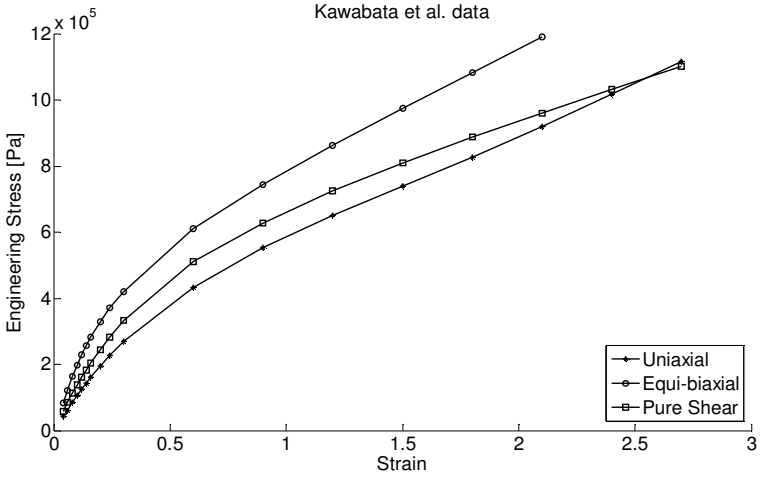

Fig. 3. Kawabata et al. data [31]

Table 1 Experimentally investigated λ values

	Treloar [27]	Kawabata et al. [31]
Uniaxial	$\lambda \in [0.0-7.5)$	$\lambda \in [0.0-3.7]$
Equi-biaxial	$\lambda \in [0.0-3.5)$	$\lambda \in [0.0-3.1]$
Pure shear	$\lambda \in [0.0-4.0)$	$\lambda \in [0.0-3.7]$

For a selected theoretical strain-energy function W we may match theoretical and experimental stress (nominal or Cauchy) in a least squares sense using data from the three cited test procedures in isolation, using any pairs of these data sets or using all the data available. That is, there are seven possible combinations of fitting W to the available experimental data. If t_i^t denotes theoretically predicted nominal stress for uniaxial $(i=1)$, equi-biaxial $(i=2)$ and pure shear $(i=3)$ and t_i^m denotes measured nominal stress, then depending upon publication read, one either minimizes:

$$E=\sum_{i=1}^{3}\beta_i\sum_{\mathbf{j=1}}^{N_i\ \mathbf{Data\ points}}\gamma_j\left[\left(t_i^m\right)_j-\left(t_i^t\left(W\left(p_1,p_2,...,p_N\right)\right)\right)_j\right]^2 \tag{12}$$

or

$$E=\sum_{i=1}^{3}\beta_i\sum_{\mathbf{j=1}}^{N_i\ \mathbf{Data\ points}}\gamma_j\left[\frac{\left(t_i^m\right)_j-\left(t_i^t\left(W\left(p_1,p_2,...,p_N\right)\right)\right)_j}{\left(t_i^m\right)_j}\right]^2. \tag{13}$$

Here β_i denotes the weighting factor applied to the distinct experimental data sets and γ_j is a weighting factor applied to a particular element of a selected experimental data set. The outer sum may be reduced if a particular form of measured data is not available. Data collected should have an equal distribution among different deformation modes at both low and high strains [40]. This is especially true if the fitting procedure uses the same weight for each experimental data [33]; however finite element method (FEM) codes, generally, use a weighting function in order to achieve a better fit near the origin (lower strains) [42].

The N simultaneously equations used to determine the strain-energy function parameters $p_i : i=1, 2, ..., N$ are formulated from $\partial E/\partial p_i = 0 : i=1, 2, ..., N$. If the system is linear a classical linear least squares technique is applied or in the case of a non linear function of the sought coefficients the Levenberg-Marquardt iterative algorithm is applied [43].

Six alternatives definitions of W are to be addressed. Details related to the fitting of Treloar [Appendix A] and Kawabata et al. data [31] for all seven possible data combinations with the five analytic forms of W is reviewed in Appendix A of the companion paper [44]. Here it is sufficient to note that use of certain data sets, in isolation or as a particular combination of data sets, do not always lead to a successful derivation of sought strain-energy functions parameters. The W functions now defined vary in number of independent variables, parameters and mathematical complexity.

2.2.2 Mathematical definition of strain-energy functions

Each analytic strain-energy function to be investigated is now briefly presented.

The Mooney–Rivlin [35] form is: $W = C_{10}(I_1 - 3) + C_{01}(I_2 - 3)$. (14)

The Ogden model [28, 29] is the most commonly used model in non-linear finite element packages [39, 40, 45]. Whilst the Ogden model is computationally more demanding than the Mooney-Rivlin model, it is preferred because it exhibits more stable fitting qualities [40]. The usual form of the Ogden strain-energy function [28, 29] is: $W = \sum_{i=1}^{N} \frac{\mu_i}{\alpha_i}\left(\lambda_1^{\alpha_i} + \lambda_2^{\alpha_i} + \lambda_3^{\alpha_i} - 3\right)$, (15)

where (μ_i, α_i) are pairs of material parameters that permit a good fit of the theoretical description to the experimental data; N is the total number of the (μ_i, α_i) pairs required. When a N-term Ogden model is used N pairs are involved and hence $2N$ material constants must be specified. Within the ABAQUS® finite element analysis (FEA) package [46] an equivalent, but slightly different, formulation for the strain-energy function is: $W = \sum_{i=1}^{N} \frac{2\mu_i}{\alpha_i^2}\left(\lambda_1^{\alpha_i} + \lambda_2^{\alpha_i} + \lambda_3^{\alpha_i} - 3\right)$. (16)

Generally a three-term Ogden model is used [45]: first term controls the low strain behaviour, the second term the high strain behaviour and the third term controls the behaviour of different deformation modes.

The Neo–Hookean model is the first constitutive mathematical model developed specifically for rubber by Treloar [27, 47]. The simple single parameter strain-energy function is:

$W = C_{10}(I_1 - 3)$. (17)

The Yeoh model [36] is essentially a generalization of Neo-Hookean model strain-energy function assuming the form: $W = C_{10}(I_1 - 3) + C_{20}(I_1 - 3)^2 + C_{30}(I_1 - 3)^3$. (18)

This model is analogous to Biderman (1958) with the linear $C_{01}(I_2 - 3)$ term removed [48].

The Arruda–Boyce or the 'eight chain' model [37] assumes the form: $W = \mu \sum_{i=1}^{5} \frac{C_i}{\lambda_m^{2i-2}}\left(I_1^i - 3^i\right)$, (19)

with coefficients assigned in accordance with:

$$C_1 = \frac{1}{2},\ C_2 = \frac{1}{20},\ C_3 = \frac{11}{1050},\ C_4 = \frac{19}{7000}\ \ \&\ \ C_5 = \frac{519}{673750}. \tag{20}$$

The coefficients $C_i : i = 1, 2, \ldots, 5$ are related to the series expansion form of the inverse Langevin function [37].

The parameters of the strain-energy function for Mooney-Rivlin, Neo-Hookean and Yeoh model have linear forms whereas the Ogden and Arruda-Boyce strain-energy functions assume non linear forms. In each case the parameters are identified by using an appropriate least-square fit solver. British Standard [26] guidance on selection of strain-energy function suggest that: Neo–Hookean is sufficient for many purposes; Yeoh and Arruda–Boyce models require a single deformation test; Mooney–Rivlin and Ogden models require a better calibration, that is, experimental data from different deformation tests.

2.2.3 Marlow model

Marlow [38] adopts a completely different approach. The strain-energy function W is defined as an integral of the stress-strain curve over the strain interval $[0, \varepsilon^*]$, that is: $W(\varepsilon^*) = \int_0^{\varepsilon^*} t_1(\varepsilon) d\varepsilon$. (21a)

Since $\varepsilon = \lambda - 1$ is the uniaxial strain and $t_1(\varepsilon)$ is the nominal uniaxial stress, it follows for uniaxial data that $I_1 = \lambda^2 + 2/\lambda$ using Equation (4a) and hence $W(\varepsilon^* = 0) = W(\lambda^* = 1) = W(I_1 = 3) = 0$, that is for λ taking any permissible value for which data exist $W(I_1)$ is simply: $W(I_1) = \int_0^{\lambda^*(I_1)-1} t_1(\varepsilon) d\varepsilon$. (21b)

Equations (21) can be used with nominal uniaxial, equi-biaxial or pure shear stress with appropriate principal stretch ratio definitions taken from Equations (4a), (9a) or (10a) respectively. This method does not seek to determine the underpinning behaviour of the material by combining all the data; it simply generates a strain-energy function for a particular set of data determined in a particular deformation mode. Marlow [38] claims that the derived W will exactly reproduce the stress strain behaviour used in the generation of W with good approximation for other deformation modes. Marlow does not claim the model is as accurate as a multi-parameter model (e.g. Ogden) when data is available in all of the basic modes. Whilst the Marlow method is readily applied its behaviour may be adversely affected if large voids occur in the data acquisition.

2.2.4 Some observations regarding strain-energy selection and rubber data

The application of strain-energy functions is widespread and the quoted alternative forms, and their variations, are used in many different research areas; in engineering [39, 40, 45], mechanical engineering [49, 50] and medical sciences research [51, 52, 53, 54]. In the static analysis of a distensible tube [13, 14, 17, 18, 21] it is sufficient to use the strain-energy forms quoted. Given the authors' observations concerning [23, 24] application of different strain-energy forms and different combinations of material strain stress data sets is necessary to identify appropriate consistent modelling techniques to provide acceptable predictions of critical pressure.

Ogden [28] suggests that good fits between theory and experimental data are achieved 'only at the expense of mathematical simplicity.' Furthermore he suggests that the generality of strain-energy functions should be achieved without being as cumbersome as the exponential forms suggested by Alexander [48] and Hart-Smith [55] or the generalized Mooney-Rivlin form expressed as:

$$W = \sum_{m,n=0}^{\infty} C_{mn}(I_1 - 3)^m (I_2 - 3)^n \quad : C_{00} = 0 .$$

Preferably the selected function should be compliant with the Valanis-Landel [56] hypothesis, namely: $W(\lambda_1, \lambda_2, \lambda_3) = f(\lambda_1) + f(\lambda_2) + f(\lambda_3)$. Valanis and Landel indicate that the variable separable form is neither arbitrary nor fortuitous, since the strain-energy function W is thought to be closely approximated by the entropy function S upon appealing to the statistical network theory of rubberlike elasticity. Furthermore, when addressing an isotropic material the entropy associated with deformation in each of the Cartesian orthogonal directions must have the same functional form with W replaced by S in the equation for $W(\lambda_1, \lambda_2, \lambda_3)$. Valanis and Landel then tested the validity of their proposal through a series of experimental investigations based on uniaxial and biaxial investigations form four distinct cited sources.

Jones & Treloar [57] observed that the Ogden formulation of Equation (15) satisfies this hypothesis. Clearly, the Neo-Hookean form of Equation (17), proposed by Treloar [27], and the simplified Mooney-Rivlin form of Equation (14) also satisfy the Valanis-Landel hypothesis.

Most of the parameters in the provided definitions of strain-energy function do not have any immediate physical interpretation. An exception is the Neo-Hookean coefficient C_{10}, which is

related to the shear modulus G. For the Ogden model, parameters α_i, μ_i of Equations (15) and (16) satisfy $G = \frac{1}{2}\sum_{i=1}^{N} \alpha_i \mu_i$ and $G = \sum_{i=1}^{N} \mu_i$ respectively.

Considering the work associated with affine deformation and the difference in entropy between the strained and unstrained states of the material Treloar [47, 58] provides arguments to demonstrate that $W = \frac{1}{2}G\left(\lambda_1^2 + \lambda_2^2 + \lambda_3^2 - 3\right)$ with $G \equiv NkT$. Here N is the number of molecules per c.c., k is the Boltzmann constant and T is the absolute temperature. It appears that, following some academic discussions presented in various journal articles, the suggestion that $G \equiv 7\,NkT/3$ by Kuhn [59] was retracted. One might argue that if the 'mathematical simplicity' of the Neo-Hookean form was sufficient then G ought to assume the same numerical value, for the same material, irrespective of the experimental data set used for its determination. According to the Treloar [27] determination of G (in 1944) using equi-biaxial data only, $G = 4.0\,kg/cm^2 \equiv 0.3924$ MPa, which gives a good fit for values of $\lambda \leq 3$, [27]. Whereas Treloar is unlikely to have used the least-squares fit method of Section 2.2.1, this procedure will yields $G =$ 0.4398 MPa (see Table A3 of [44]). A least squares fit of first and second Ogden models respectively yield $G = 0.4270$ MPa and $G = 0.4338$ MPa. The uniaxial or pure shear data sets provide G values completely inconsistent with the previous equi-biaxial derived values. To quote Treloar [27]: *'The reason for the departures from the theoretical form in the cases of elongation and shear is not obvious*.' In other words different G values are required to best fit each distinct experimental data set (see Figure 2). Despite the 'mathematical simplicity' of some strain-energy functions each model will be applied in the finite element analysis of a tube undergoing an aneurysm. This apparently irrational step is taken because in certain applications the observed mathematical simplicity always yields a stable finite element formulation, whereas more complex function forms can be unstable. The manner in which numerical instability arises is highlighted in Appendix A of [44].

Having addressed some of the nuances of fitting strain-energy functions to experimental data the next section provides the theoretical background to alternative methods of investigating aneurysm onset and growth.

3. Alternative methods for prediction of aneurysm related critical pressure

Three radically different approaches are applied to determine critical pressure. The first two choices are semi-analytic whereas the third choice is a finite element approach applicable to incompressible materials. The simplest method of Section 3.1 merely seeks the variation of inflation pressure with uniform longitudinal radial growth of tube, as measured by λ_1. For a selected λ_1-value the corresponding longitudinal extension λ_2 is determined iteratively subject to satisfaction of the longitudinal equilibrium condition using a bisection method for each selected function W. Thereafter the equation of radial equilibrium is used to determine the required inflation pressure for the identified combination of λ_1- and λ_2-values. The more advanced method of Section 3.2 seeks indirect solution of a set of four ordinary governing differential equations describing the quasi static-equilibrium of an axisymmetric membrane. The original two point boundary value problem is converted into an initial value problem that is solved applying a 'shooting' technique. Cited papers [14, 17, 18] quote the details of the boundary value problem formulation without specific derivation or source details. Hence an outline derivation is provided since the authors have failed to locate a publication providing required derivations. The last method of Section 3.3 is the finite element method. The fundamental and theoretical concepts required in the context of a hyper-elastic material are addressed with a discussion of the specific solution method selected in the analysis application.

All the methods are to be tested for different strain-energy functions using the seven different possible combinations of available experimental data sets provide by Treloar and Kawabata et al.

3.1 Critical pressure prediction for a long thin-walled tube

The semi-analytic method to be presented is essentially a means of cross-checking critical pressure. This approach does not address the longitudinal variation of the tube cross sectional shape as the aneurysm continues development. That is, the changes determined for any one transverse section of the tube is a description of how the whole tube changes uniformly along its length.
In Section 2 Equations (4a), (9a) and (10a) provide specific behavioural characteristics for λ_1, λ_2 and λ_3 in accordance with the particular experimental method of measuring stress. The physical condition now considered is the inflation of a long and thin circular tube of initial length l_0, initial radius r_0 and wall thickness t_{w0}. In this case λ_1 is the circumferential or azimuthal stretch, r/r_0 and

λ_2 is the axial or meridional stretch, l/l_0. For an incompressible isotropic rubber the Cauchy stress is as specified in Equation (3). With $W = W(I_1, I_2)$ and strain invariants defined in Equation (2), application of the chain rule in Equation (3) readily leads to:

$$\sigma_i = 2\left[\lambda_i^2 \frac{\partial W}{\partial I_1} - \frac{1}{\lambda_i^2}\frac{\partial W}{\partial I_2}\right] - p \quad : i = 1, 2 \,\&\, 3. \tag{22}$$

Since the rubber tube has a thin wall $\sigma_3 = 0$ is assumed. Hence p can be eliminated from σ_1 and σ_2 to yield:

$$\sigma_i = 2\left[\lambda_i^2 \frac{\partial W}{\partial I_1} - \frac{1}{\lambda_i^2}\frac{\partial W}{\partial I_2}\right] - 2\left[\frac{1}{(\lambda_1\lambda_2)^2}\frac{\partial W}{\partial I_1} - (\lambda_1\lambda_2)^2\frac{\partial W}{\partial I_2}\right] : i = 1 \,\&\, 2. \tag{23}$$

That is, in agreement with [15]:

$$\sigma_1 = 2\left[\lambda_1^2 - \frac{1}{(\lambda_1\lambda_2)^2}\right]\left[\frac{\partial W}{\partial I_1} + \lambda_2^2\frac{\partial W}{\partial I_2}\right] \tag{24a}$$

and

$$\sigma_2 = 2\left[\lambda_2^2 - \frac{1}{(\lambda_1\lambda_2)^2}\right]\left[\frac{\partial W}{\partial I_1} + \lambda_1^2\frac{\partial W}{\partial I_2}\right]. \tag{24b}$$

Since the Ogden model is not expressed in terms of I_1 and I_2, but uses directly the stretch ratios, alternative equivalent expressions for σ_1 and σ_2 are required. Reverting to Equation (3) and substituting for p in σ_1 and σ_2, using $\sigma_3 = 0$, immediately leads to:

$$\sigma_1 = \lambda_1\frac{\partial W}{\partial \lambda_1} - \lambda_3\frac{\partial W}{\partial \lambda_3} \tag{25a}$$

and

$$\sigma_2 = \lambda_2\frac{\partial W}{\partial \lambda_2} - \lambda_3\frac{\partial W}{\partial \lambda_3}. \tag{25b}$$

The radial equilibrium condition [60] was originally discovered by Mariotte [61]. Mariotte became one of the first members of the French Academy of Science, in 1666, and was largely responsible for the introduction of experimental method into French science. Mariotte designed the pipelines to supply water to the Palace of Versailles and subsequently discovered experimentally the bursting strength of pipes under internal hydrostatic pressure. He deduced that the required thickness of pipe must be proportional to the internal pressure and the pipe diameter [61]. Mariotte observations for a tube of radius r, thin wall thickness t_w, and an assumed inflation pressure P led to the circumferential equilibrium equation:

$$\sigma_1 t_w = P\,r \;\text{ or }\; \sigma_1 = P\frac{r}{t_w}. \tag{26a}$$

From the definition of λ_1 it follows that $r = \lambda_1 r_0$, whereas the incompressibility of the material requires that $t_{w0} = \lambda_1\lambda_2 t_w$, and hence the radial equilibrium condition takes the form:

$$\sigma_1 = P\lambda_1^2\lambda_2\frac{r_0}{t_{w0}}, \tag{26b}$$

with subscript '0' indicating an undeformed dimension. The longitudinal equilibrium requires that:

$$\sigma_2 = \frac{P\,r}{2t_w} = \frac{\sigma_1}{2}. \tag{27}$$

Hence from Equation (27) and Equations (24a) and (24b) it follows that:

$$\left[\lambda_1^2 - 2\lambda_2^2 + \frac{1}{(\lambda_1\lambda_2)^2}\right]\frac{\partial W}{\partial I_1} + \left[\frac{2}{\lambda_2^2} - \frac{1}{\lambda_1^2} - (\lambda_1\lambda_2)^2\right]\frac{\partial W}{\partial I_2} = 0, \tag{28a}$$

or, using Equation (27) with Equations (25a) and (25b) yields:

$$\lambda_1\frac{\partial W}{\partial \lambda_1} - 2\lambda_2\frac{\partial W}{\partial \lambda_2} + \lambda_3\frac{\partial W}{\partial \lambda_3} = 0 \;\text{ with }\; \lambda_3 = \frac{1}{\lambda_1\lambda_2}. \tag{28b}$$

Equations (28) provide a general relation between hoop (σ_1) and axial (σ_2) stresses for an arbitrary given strain-energy function W expressed in terms of the strain invariant derivatives (28a) or the stretch ratio derivatives (28b). With Equations (28) provided, a plot of P versus λ_1 can be obtained as follows:

- Select λ_1-value and solve Equation (28a) for λ_2 using any of the cited functions W other than the Ogden form. For an Ogden formulation Equation (28b) is used to determine λ_2.
- Use λ_1- and λ_2-values and known gradients of W to determine σ_1 using Equations (24a) or (25a) depending upon W selected.
- Use derived σ_1 for determined λ_1- and λ_2-values to provide P using Equation (26b).

This algorithm appears to be consistent with a procedure outlined by [13]. The nonlinear Equation (28a), according to the selected strain-energy function assumes the following forms:

Neo-Hookean: $$C_{10}\left[2\lambda_2^4 - \lambda_1^2\lambda_2^2 - \frac{1}{\lambda_1^2}\right] = 0, \tag{29NH}$$

Mooney-Rivlin: $$\lambda_2^4\left[C_{01}\lambda_1^4 + 2C_{10}\lambda_1^2\right] + \lambda_2^2\left[C_{01} - C_{10}\lambda_1^4\right] - \left[C_{10} + 2\lambda_1^2 C_{01}\right] = 0, \tag{29MR}$$

Yeoh: $$\left[\lambda_1^2 - 2\lambda_2^2 + \frac{1}{(\lambda_1\lambda_2)^2}\right]\left[C_{10} + 2C_{20}(I_1 - 3) + 3C_{30}(I_1 - 3)^2\right] = 0, \tag{29Y}$$

and

Arruda-Boyce: $$\mu\left[\lambda_1^2-2\lambda_2^2+\frac{1}{\left(\lambda_1\lambda_2\right)^2}\right]\sum_{i=1}^{5}iC_i\left(\frac{I_1}{\lambda_m^2}\right)^{i-1}=0\,, \tag{29AB}$$

whereas Equation (28b) for Ogden has the generalized form

$$\begin{aligned}&\lambda_1\left[\mu_1^m\lambda_1^{\alpha_1-1}+\mu_2^m\lambda_1^{\alpha_2-1}\delta_{m2}+\mu_3^m\lambda_1^{\alpha_3-1}\delta_{m3}\right]-2\lambda_2\left[\mu_1^m\lambda_2^{\alpha_1-1}+\mu_2^m\lambda_2^{\alpha_2-1}\delta_{m2}+\mu_3^m\lambda_2^{\alpha_3-1}\delta_{m3}\right]+\\&\lambda_3\left[\mu_1^m\lambda_3^{\alpha_1-1}+\mu_2^m\lambda_3^{\alpha_2-1}\delta_{m2}+\mu_3^m\lambda_3^{\alpha_3-1}\delta_{m3}\right]=0.\end{aligned} \tag{29OG}$$

In Equation (29OG) a generic mth order Ogden model is assumed and the Krönecker delta functions satisfy: (i) $\delta_{m2}=1$ if $m\geq 2$ and 0 otherwise, (ii) $\delta_{m3}=1$ if $m=3$ and 0 otherwise.

Each form of the nonlinear Equation (29) was solved for λ_2 for each selected λ_1-value. The Neo-Hookean form (29NH) is readily solved in closed analytic form, whereas all other forms are solved using a bisection method. Since the behaviour of $f\left(\lambda_2\mid\lambda_1\right)$ for each form of the left hand side of Equation (29) is quite distinct a selected relative error convergence tolerance must reflect the range and gradient values of this function $f\left(\lambda_2\mid\lambda_1\right)$. For λ_1-values generally greater than 5 the Yeoh model requires more care than the other models due to excessive steep gradients of $f\left(\lambda_2\mid\lambda_1\right)$. This means the relative error threshold (usually 10^{-3}) cannot be so refined. A suitable convergence tolerance was selected for each model to reflect the numerical range of function values.

A representative selection of results based on the application of this technique will be presented and discussed in Section 4.1. Next, we provide a more sophisticated semi-analytic analysis capable of identify both critical pressure and longitudinal variation of the tube geometry as aneurysm develops.

3.2 Critical pressure prediction for an axisymmetric membrane of finite length

The previous method assumed the tube maintained the same circular cross-section longitudinally whilst expanding as pressure increased. In the method now formulated this assumption is relaxed. The physical problem is the inflation of an axisymmetric membrane using an appropriate set of ordinary differential equations. The governing equations are derived by manipulating geometric relationships and equilibrium conditions through the use of strain-energy function W to provide expressions for the traction forces. Derivations are provided in outline form since no publication of their origin has been located.

With x and s defined as the axial and curvilinear coordinates of tube, and subscript ‘0’ indicating an original state, the stretch parameters satisfy:

$$\lambda_1 = \frac{r}{r_0}, \quad \lambda_2 = \frac{ds}{ds_0} \text{ and } \lambda_3 = \frac{t_w}{t_{w0}} \equiv \frac{1}{\lambda_1 \lambda_2}. \tag{30}$$

The principal curvatures in the circumferential and axial directions are defined as:

$$\kappa_1 = \frac{\cos\theta}{r} \text{ and } \kappa_2 = \frac{d\theta}{ds}. \tag{31}$$

The following geometric relationships can be deduced from Figure 4a:

$$\frac{dr}{ds} = -\sin\theta \text{ and } \frac{dx}{ds} = \cos\theta. \tag{32}$$

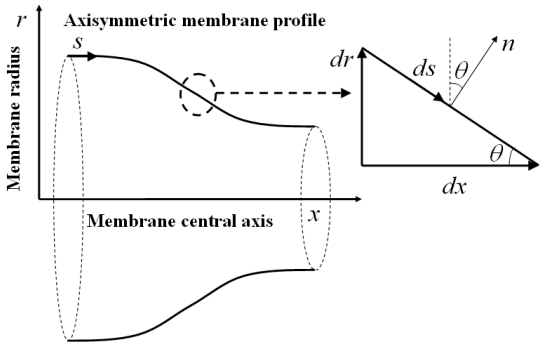

Fig. 4a. Geometric relationship between x, r, s and θ

The circumferential (azimuthal) and the axial (meridional) principal stress resultants T_1 & T_2 illustrated in Figure 4b, are defined as:

$$T_1 = t_w[\sigma_1 - \sigma_3] \equiv t_w \lambda_1 \frac{\partial \hat{W}}{\partial \lambda_1} = \frac{t_{w_0}}{\lambda_2} \frac{\partial \hat{W}}{\partial \lambda_1} \text{ and } T_2 = t_w[\sigma_2 - \sigma_3] \equiv t_w \lambda_2 \frac{\partial \hat{W}}{\partial \lambda_2} = \frac{t_{w_0}}{\lambda_1} \frac{\partial \hat{W}}{\partial \lambda_2}. \tag{33}$$

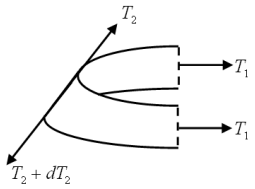

Fig. 4b. Definition of directions of stress resultants T_1 and T_2 ([62])

The Laplace equilibrium condition [62]:

$$\kappa_1 T_1 + \kappa_2 T_2 = P, \tag{34}$$

is readily appreciated through Figure 4c.

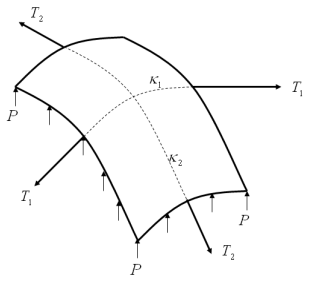

Fig. 4c. Representation of Laplace equilibrium equation (based on [62])

Equations (30) to (34) are basic equations that are to be utilized with an additional equation representing the quasi-static equilibrium of deformation of a membrane. Initially we sought utilization of Equation (12) in Guo [17], namely:

$$\frac{dT_2}{dx} + (T_2 - T_1)\frac{d}{dx}\left[\ln(\lambda_1 r_0)\right] = 0\,, \tag{35a}$$

prior to realizing that the logarithmic term is incorrectly dimensional. Figure 4d readily permits demonstration of the veracity of Equation (8a) in Kyriakides & Chang [14], namely:

$$2\pi r_0 \lambda_1 T_2 \cos\theta = \pi r_0^2 \lambda_1^2 P\,. \tag{35b}$$

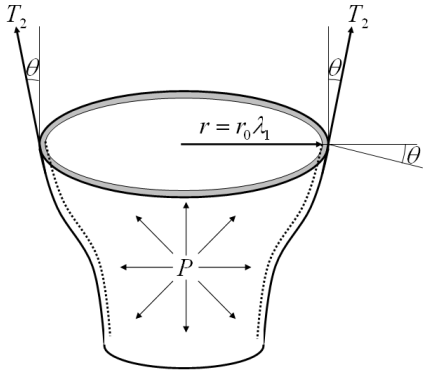

Fig. 4d. Representation of Kyriakides & Chang equilibrium equation

However, using Equation (35b) as a starting point the authors failed to derive the final set of governing differential equations used by Guo [17,18] and Kyriakides & Chang [14] in their theoretical studies. Finally, noting that both Green & Adkins [63] and Guo [18] suggest the same alternative form of equilibrium equation, namely:

$$\frac{d(T_2 r)}{ds} = T_1 \frac{dr}{ds}, \tag{35c}$$

this equation was successfully used to derive the remaining required governing equation quoted in each of the studies [14, 17, 18]. It should be noted that indices 1 and 2 in Equations (35) are

interchanged in the original cited sources. Derivation of the governing equations, considered next, is limited to the necessary principal steps.

3.2.1 Outline derivation of governing equations

From the chain rule $\frac{dx}{dx_0} = \frac{dx}{ds}\frac{ds}{ds_0}\frac{ds_0}{dx_0}$ and definitions of λ_2 and dx/ds, provided in Equations (30) and (32), it follows that: $\frac{dx}{dx_0} = \lambda_2 \cos\theta \frac{ds_0}{dx_0}$. (36a)

Applying an appropriate chain rule to the derivative $d\lambda_1/dx_0$ leads to:

$$\frac{d\lambda_1}{dx_0} \equiv \frac{d}{dx_0}\left(\frac{r}{r_0}\right) = \frac{1}{r_0^2}\left[r_0 \frac{dr}{ds}\frac{ds}{ds_0}\frac{ds_0}{dx_0} - \frac{dr_0}{dx_0} r\right].$$

Definitions of λ_1 & λ_2 and dr/ds of Equations (30) and (32) simplify the last equation to:

$$\frac{d\lambda_1}{dx_0} = -\frac{1}{r_0}\left[\lambda_2 \sin\theta \frac{ds_0}{dx_0} + \lambda_1 \frac{dr_0}{dx_0}\right]. \quad (36b)$$

Substituting into Equation (34) the expressions for the principal resultants stresses T_1 and T_2, provided in Equation (33), together with definitions of principal curvatures κ_1 and κ_2 of Equation (31), yields: $\frac{\cos\theta}{r} t_w \lambda_1 \frac{\partial \hat{W}}{\partial \lambda_1} + \frac{d\theta}{ds} t_w \lambda_2 \frac{\partial \hat{W}}{\partial \lambda_2} = P$.

Use of $\hat{W} = \hat{W}(\lambda_1, \lambda_2)$ recognizes dependence of λ_3 upon λ_1 and λ_2 within the general form $W = W(\lambda_1, \lambda_2, \lambda_3)$. Dividing the last derived equation by t_w, applying the chain rule $\frac{d\theta}{ds} \equiv \frac{d\theta}{dx_0}\frac{dx_0}{ds_0}\frac{ds_0}{ds}$ and recalling definitions of λ_1, λ_2 and λ_3 from Equation (30) permits derivation of third governing equation: $\frac{d\theta}{dx_0} = \frac{ds_0}{dx_0}\frac{1}{\frac{\partial \hat{W}}{\partial \lambda_2}}\left[\frac{\lambda_1 \lambda_2}{t_{w0}} P - \frac{\cos\theta}{r_0}\frac{\partial \hat{W}}{\partial \lambda_1}\right]$. (36c)

Finally to complete the derivation of the frequently quoted governing equations [14, 17, 18] Equation (35c) is readily re-expressed in the form: $r\frac{dT_2}{ds} = (T_1 - T_2)\frac{dr}{ds}$.

Replacing $\frac{dT_2}{ds}$ with $\frac{dT_2}{dx_0}\frac{dx_0}{ds}$ and undertaking the operation $\frac{dT_2}{dx_0} \equiv \left[\frac{\partial T_2}{\partial \lambda_1}\frac{d\lambda_1}{dx_0} + \frac{\partial T_2}{\partial \lambda_2}\frac{d\lambda_2}{dx_0}\right]$ yields:

$$r\left[\frac{\partial T_2}{\partial \lambda_1}\frac{d\lambda_1}{dx_0} + \frac{\partial T_2}{\partial \lambda_2}\frac{d\lambda_2}{dx_0}\right]\frac{dx_0}{ds} = (T_1 - T_2)\frac{dr}{ds}.$$

Next substituting for T_1 & T_2, using Equation (33), and completing the operations $\partial(\ )/\partial\lambda_1$ and $\partial(\ )/\partial\lambda_2$ leads to: $r\left[\frac{1}{\lambda_1}\frac{\partial^2\hat{W}}{\partial\lambda_1\partial\lambda_2}\frac{d\lambda_1}{dx_0}-\frac{1}{\lambda_1^2}\frac{\partial\hat{W}}{\partial\lambda_2}\frac{d\lambda_1}{dx_0}+\frac{1}{\lambda_1}\frac{\partial^2\hat{W}}{\partial\lambda_2^2}\frac{d\lambda_2}{dx_0}\right]\frac{dx_0}{ds}=\left(\frac{1}{\lambda_2}\frac{\partial\hat{W}}{\partial\lambda_1}-\frac{1}{\lambda_1}\frac{\partial\hat{W}}{\partial\lambda_2}\right)\frac{dr}{ds}$,

upon cancellation of the common term t_{w_0}. Rearranging terms and multiplying by ds/ds_0, recalling the definition of λ_1 and substituting for $d\lambda_1/dx_0$ using Equation (36b), provides:

$$r_0\frac{\partial^2\hat{W}}{\partial\lambda_2^2}\frac{d\lambda_2}{dx_0}=\left(\frac{1}{\lambda_2}\frac{\partial\hat{W}}{\partial\lambda_1}-\frac{1}{\lambda_1}\frac{\partial\hat{W}}{\partial\lambda_2}\right)\frac{dr}{ds}\frac{ds}{dx_0}-\frac{r}{\lambda_1}\frac{\partial^2\hat{W}}{\partial\lambda_1\partial\lambda_2}\left(-\frac{1}{r_0}\left[\lambda_2\sin\theta\frac{ds_0}{dx_0}+\lambda_1\frac{dr_0}{dx_0}\right]\right)$$
$$+\frac{r}{\lambda_1^2}\frac{\partial\hat{W}}{\partial\lambda_2}\left(-\frac{1}{r_0}\left[\lambda_2\sin\theta\frac{ds_0}{dx_0}+\lambda_1\frac{dr_0}{dx_0}\right]\right).$$

Expanding terms within square brackets and applying definitions of λ_1, λ_2 and dr/ds of Equations (30) and (32) simplifies the last equation to read:

$$r_0\frac{\partial^2\hat{W}}{\partial\lambda_2^2}\frac{d\lambda_2}{dx_0}=\left(\frac{1}{\lambda_2}\frac{\partial\hat{W}}{\partial\lambda_1}-\frac{1}{\lambda_1}\frac{\partial\hat{W}}{\partial\lambda_2}\right)\frac{dr}{ds}\frac{ds}{dx_0}+\frac{\partial^2\hat{W}}{\partial\lambda_1\partial\lambda_2}\lambda_2\sin\theta\frac{ds_0}{dx_0}-\frac{r}{\lambda_1}\frac{\partial^2\hat{W}}{\partial\lambda_1\partial\lambda_2}\left(-\frac{1}{r_0}\lambda_1\frac{dr_0}{dx_0}\right)$$
$$+\frac{1}{\lambda_1}\frac{\partial\hat{W}}{\partial\lambda_2}\frac{dr}{dx_0}-\frac{\partial\hat{W}}{\partial\lambda_2}\frac{dr_0}{dx_0}.$$

Observing that the second part of the first term is cancelled by the penultimate term of the last equation, implying:

$$r_0\frac{\partial^2\hat{W}}{\partial\lambda_2^2}\frac{d\lambda_2}{dx_0}=\left(\frac{1}{\lambda_2}\frac{\partial\hat{W}}{\partial\lambda_1}\frac{dr}{ds}\frac{ds}{dx_0}\right)+\frac{\partial^2\hat{W}}{\partial\lambda_1\partial\lambda_2}\lambda_2\sin\theta\frac{ds_0}{dx_0}-\frac{r}{\lambda_1}\frac{\partial^2\hat{W}}{\partial\lambda_1\partial\lambda_2}\left(-\frac{1}{r_0}\lambda_1\frac{dr_0}{dx_0}\right)-\frac{\partial\hat{W}}{\partial\lambda_2}\frac{dr_0}{dx_0}.$$

Substituting for dr/ds and simplifying other terms, using definition of λ_1, provides (with minor rearrangements) the required governing equation:

$$\frac{d\lambda_2}{dx_0}=\frac{1}{r_0}\frac{1}{\dfrac{\partial^2\hat{W}}{\partial\lambda_2^2}}\left[\left(\frac{\partial^2\hat{W}}{\partial\lambda_1\partial\lambda_2}\lambda_2-\frac{\partial\hat{W}}{\partial\lambda_1}\right)\frac{ds_0}{dx_0}\sin\theta+\left(\frac{\partial^2\hat{W}}{\partial\lambda_1\partial\lambda_2}\lambda_1-\frac{\partial\hat{W}}{\partial\lambda_2}\right)\frac{dr_0}{dx_0}\right]. \tag{36d}$$

Equations (36) represent a system of non-linear first order differential equations to be solved for λ_1, λ_2, x and θ assuming P is known. Apart from notation changes this equation agrees with Guo [17]. Other than implicit definition of pressure these equations are consistent with that of Kyriakides & Chang [14] upon setting their axial force to zero.

The required derivatives of the strain-energy function $W(\lambda_1,\lambda_2,\lambda_3)\equiv\hat{W}(\lambda_1,\lambda_2)$, defined in Section 2.2.2, are stated in Appendix B.

3.2.2 Solution of governing equations

Assuming the tube has an initial length of $2l_0$ and the tube is not allowed to extend in the axial direction, the boundary conditions at the central location and end point of the tube are

$$x\big|_{x_0=0} = 0 \quad \& \quad \theta\big|_{x_0=0} = 0 \tag{37a}$$

and

$$x\big|_{x_0=l_0} = l_0 \quad \& \quad \lambda_1\big|_{x_0=l_0} = 1. \tag{37b}$$

The first two conditions define the symmetry conditions at the centre of the tube, whereas the second pair of conditions require the end of the tube to remain fixed and the cross sectional area to be unchanged. Since the rubber tube has an initial cylindrical shape of uniform section then it follows that $dr_0/dx_0 = 0$ and $ds_0/dx_0 = 1$ and hence Equations (36) can be simplified to the form presented by Guo [18], that is

$$\frac{dx}{dx_0} = \lambda_2 \cos\theta, \tag{38a}$$

$$\frac{d\lambda_1}{dx_0} = -\frac{1}{r_0}\lambda_2 \sin\theta, \tag{38b}$$

$$\frac{d\theta}{dx_0} = \frac{1}{\dfrac{\partial \hat{W}}{\partial \lambda_2}}\left[\frac{\lambda_1\lambda_2}{t_{w0}}P - \frac{\cos\theta}{r_0}\frac{\partial \hat{W}}{\partial \lambda_1}\right] \tag{38c}$$

and

$$\frac{d\lambda_2}{dx_0} = \frac{1}{r_0}\frac{1}{\dfrac{\partial^2 \hat{W}}{\partial \lambda_2^2}}\left(\frac{\partial^2 \hat{W}}{\partial \lambda_1 \partial \lambda_2}\lambda_2 - \frac{\partial \hat{W}}{\partial \lambda_1}\right)\sin\theta. \tag{38d}$$

The two-point boundary value problem of Equations (38) subject to boundary conditions (37) is next re-cast as an initial value problem. In this case the boundary conditions (37a), at the tube centre, are treated as two initial conditions. Two additional fictitious initial conditions are

$$\lambda_2\big|_{x_0=0} = \lambda_2^* \quad \& \quad P\big|_{\forall x} = P^*. \tag{39}$$

Thereafter Equations (38) are solved subject to initial conditions (37a) and (39). If the solution fails to satisfy conditions (37b) then λ_2^* and P^*, of Equation (39), are modified until (37b) is satisfied. The solution technique outlined is often referred to as a 'shooting' technique [19].

Application of the simpler method of Section 3.1 suggests (for the selected rubber models) that an aneurysm is initiated when $\lambda_1 \in$ (1.6, 1.9). The corresponding required $\lambda_2 \in$ (1.05, 1.25). For compatible λ_1- and λ_2-values the critical pressure was typically 27-38 kPa, depending on combination of data sets used to identify parameters of selected strain-energy function W. Guo [17] suggested formulae for selecting the initial values of λ_2^* and P^* were less successful here than in his medical application.

3.2.3 Algorithm implemented

The shooting technique was implemented in accordance with the following procedure:

- A sensible range of λ_1-values is selected in order to provide a range of pressure values that includes the critical pressure. The initial variation of pressure versus radial stretch (λ_1) is generally linear in behaviour (from observation). Experience of application of this approach suggested reduced numerical effort was achieved by exploiting our observations and using $\lambda_1 = 1.3$ as the initial value in the task of identifying the λ_1-value associated with the occurrence of critical pressure.
- For a selected λ_1-value, initial values of λ_2^* and P^* are assigned in accordance with $\lambda_2^* = \eta_\lambda \lambda_1$ and $P^* = \eta_P P^{critical}$. The coefficients satisfy $\eta_\lambda = 1.15$ and $\eta_P = 0.8$. $P^{critical}$ is selected from application of the simpler method outline in Section 3.1.
- Equations (38) are solved for specified (λ_2^*, P^*) values using a specific Matlab® implemented fourth-fifth order Runge-Kutta solver (ode45) [64]. Satisfaction of the boundary conditions (37b) is then checked for an absolute difference tolerance of the order of $|10^{-6}|$.
- If the initial pair of values (λ_2^*, P^*) does not lead to satisfaction of (37b), then Equations (38) are next solved for the following 4 pairs of shooting parameters: $(\lambda_2^* + \Delta\lambda_2, P^*)$, $(\lambda_2^* - \Delta\lambda_2, P^*)$, $(\lambda_2^*, P^* + \Delta P)$ & $(\lambda_2^*, P^* - \Delta P)$. Thereafter the errors E_{λ_1} and E_x are evaluated by comparing required condition (37b) with actual derived end conditions. The errors E_{λ_1} and E_x associated with the first and second pair, and the third and fourth pair, of suggested shooting parameters permit estimated values of:

  $\left.\frac{\partial E_{\lambda_1}}{\partial \lambda_2}\right|_{(\lambda_2^*, P^*)}$, $\left.\frac{\partial E_x}{\partial \lambda_2}\right|_{(\lambda_2^*, P^*)}$ and $\left.\frac{\partial E_{\lambda_1}}{\partial P}\right|_{(\lambda_2^*, P^*)}$, $\left.\frac{\partial E_x}{\partial P}\right|_{(\lambda_2^*, P^*)}$ respectively.

- The Jacobian of estimated error gradients is readily defined as:

$$J = \begin{bmatrix} \left.\dfrac{\partial E_{\lambda_1}}{\partial \lambda_2}\right|_{(\lambda_2^*, P^*)} & \left.\dfrac{\partial E_{\lambda_1}}{\partial P}\right|_{(\lambda_2^*, P^*)} \\ \left.\dfrac{\partial E_x}{\partial \lambda_2}\right|_{(\lambda_2^*, P^*)} & \left.\dfrac{\partial E_x}{\partial P}\right|_{(\lambda_2^*, P^*)} \end{bmatrix} \tag{40a}$$

and the required changes $(\delta\lambda_2^*, \delta P^*)$ to current estimates (λ_2^*, P^*) are determined from:

$$\begin{Bmatrix} \delta\lambda_2^* \\ \delta P^* \end{Bmatrix} = J^{-1} \begin{Bmatrix} dE_{\lambda_1} \\ dE_x \end{Bmatrix}. \tag{40b}$$

- New parameter values $(\lambda_2^{*(i+1)}, P^{*(i+1)})$ are assigned in accordance with $\lambda_2^{*(i+1)} = \lambda_2^{*(i)} + \omega\delta\lambda_2^*$ and $P^{*(i+1)} = P^{*(i)} + \omega\delta P^*$. Here i indicates current iteration number and ω is a relaxation factor used to control convergence of the shooting method.
- Recasting original boundary value problem as an initial value problem does not guarantee that convergence of the process is a straight forward procedure. This is certainly the case in addressing Equations (38). The adopted approach may be summarized as follows:
  - Typical initial value of ω is 0.5.
  - When λ_1 is increased from $\lambda_1^{(n)}$ to $\lambda_1^{(n+1)}$ then λ_2 is expected to increase and P can increase or decrease depending upon whether P is below or above critical pressure. Relaxation factor ω is lowered and solution restarted when the current i^{th}-iterated value of the shooting parameters $\lambda_2^{(n+1)_i}$ or $P^{(n+1)_i}$ does not satisfy $1 \le \left(\lambda_2^{(n+1)_i} / \lambda_2^n\right) \le 1.5$ or $0.8 \le \left(P^{(n+1)_i} / P^n\right) \le 1.4$ respectively. These inequalities are dependent upon the converged values of the parameters of the previous n^{th} step, or, the initial assigned values for $n = 1$.
  - If one or both parameters lie outside the inequality limits, it is considered self evident that the current state of solution is not physically meaningful. Therefore the process needs to be restarted. This may be achieved by restarting the process with the same initial values but with the relaxation factor ω reduced by 10%. If there is a further failure the relaxation is repeatedly reduced by 10% until convergence is achieved, or, the total number of iterations for the current λ_1-value exceeds a threshold. This threshold unfortunately is influenced by the selected strain-energy function. Upon exceeding the selected threshold a final attempt is initiated by using the initial values of (λ_2^*, P^*) with the last relaxation factor ω, prior to threshold

exceedence failure, assigned. If both these alternative strategies fail this particular λ_1-value is abandoned.

- When boundary condition (37b) is satisfied for current λ_1, then λ_1 is incremented by 0.01 and the process is repeated until the whole required range of λ_1-values is investigated.

This approach might be considered to have a rather complex associated algorithm. In other papers [17, 18] using the shooting method there is no discussion of the implementation details. The nuances addressed were found necessary since the process was applied to tubes of significantly larger aspect ratio, $2l_0/r_0$ than the other cited publications [17, 18]. In fact as this ratio increases the numerical effort required increases.

In common with the procedure outlined in Section 3.1, representative results from application of this method are presented and discussed in Section 4.2. Having provided two distinct critical pressure assessment procedures of differing complexity we next consider the finite element approach.

3.3 Selection of finite element formulation

The classical displacement-based finite element formulation is well established in many commercial finite element codes. The results provided are generally accurate. An exception occurs for problems involving an incompressible rubber-like material. In this case a mixed finite element formulation is required to avoid 'locking' problems. Structural analysis affected by locking seems to enlarge structural stiffness and consequently the displacements and hence strains and stresses are underestimated. 'Locking' can arise in many different situations [41]. The algebraic system associated with a finite element discretisation can become ill-conditioned. For an incompressible material, such as rubber, the 'volumetric locking' effect is attributed to the Poisson ratio approaching the thermodynamic limit of 0.5.

Volumetric locking may be overcome by adopting one of the following approaches:

- Mixed displacement-pressure formulation (U/P): the unknowns variables are represented by displacements and pressure [65].
- Enhanced strain method: element formulation is enriched with strain modes in order to have better predictive capabilities [66, 67].

- Mixed penalty formulation: the introduction of a penalty parameter is used to perturb the divergence free constraint [68].

The U/P mixed formulation is the most efficient technique [69, 70]. Furthermore, this formulation is free from both 'checker-board' pressure modes [71] and 'hour-glass' deformation modes that occurs in the enhanced strain method used for large strain conditions [69] or when reduced integration is used [72]. For an incompressible material a U/P hybrid method is recommended [73]. Whilst useful information concerning different elements [40] is available, only 2D and 3D solid element based U/P formulations are available in commercial FEA packages. An evolution of the MITC4[1] shell element [41] awaiting commercialization is the MITC4–3D shell element developed by Toscano & Dvorkin [74]. This can model hyper-elastic materials. Having justified selection of the U/P mixed formulation, the formulation is briefly introduced together with the impact of the strain-energy function upon the creation of the stiffness matrix.

3.3.1 U/P mixed formulation

This section is primarily concerned with how the strain-energy is taken into account within the FEA formulation. Without undertaking a first principles approach it is sufficient to state that the finite element formulation is generally obtained by using the principle of virtual work, whereby the internal virtual work is considered to be in equilibrium with the external virtual work. Physically this means that the external loads applied deform the body and consequently stresses are developed within the material (as an internal reaction) to obtain a state of equilibrium. A more general mathematical approach to the derivation of the finite element formulation is to recast the governing differential (strong) equations into their integral (weak) form [72].

The finite element counterpart of the internal work is represented by the stiffness matrix. In formulating the U/P approach the stress tensor is partitioned into the deviatoric and volumetric parts; the deviatoric stress leads to a stiffness matrix designated $\mathbf{K}_{uu}$ and the volumetric stress leads to the stiffness matrix $\mathbf{K}_{up}$. The sub-matrices $\mathbf{K}_{pu}$ and $\mathbf{K}_{pp}$ of the stiffness matrix arise from the weak form of the equation that relates pressure p to the volumetric strain ε_v via the bulk modulus κ, i.e. $p = -\kappa\varepsilon_v$.

Throughout this paper numerical simulations performed are static (not dynamic) leading to a simplified formulation in which the mass matrix is neglected. This static analysis strategy is also

[1] A four node Mixed Interpolation of Tensorial Components (MITC)

used to assess the rupture of a developed abdominal aortic aneurysm in [75, 76, 77] and the value of systolic pressure is applied statically.

The U/P formulation [41, 78] assumes the form:

$$\begin{bmatrix} \mathbf{K}_{uu} & \mathbf{K}_{up} \\ \mathbf{K}_{pu} & \mathbf{K}_{pp} \end{bmatrix} \begin{Bmatrix} \overline{\mathbf{U}} \\ \overline{\mathbf{P}} \end{Bmatrix} = \begin{Bmatrix} \mathbf{R} \\ 0 \end{Bmatrix}, \tag{41}$$

where $\mathbf{R}$ is the external load vector and $\mathbf{K}$ is the stiffness matrix. The displacement (u) and pressure (p) constitute the primitive variables of the formulation. The $\mathbf{K}_{pp}$ part of the stiffness matrix is identically zero if the material is totally incompressible. This formulation can be extended to take into account a non-linear elasticity effect, using an incremental formulation [79]. In this case the whole displacement field is solved as a sequence of equilibrium configurations (steps) through the introduction of a fictitious time.

The actual configuration at time $t+\Delta t$ is unknown and hence external forces, stresses and strains are assigned in accordance with two possible approaches. In the total Lagrangian formulation the stresses and strains are related to the initial (undeformed) configuration. In the alternative updated Lagrangian formulation the stresses and strains are determined from the previous artificial time step. In each case the resulting stress tensors are respectively designated second Piola-Kirchhoff and Cauchy, whereas the strain tensors are referred to as Green-Lagrange and infinitesimal strain respectively [80]. For an appropriate and meaningful definition of energy stored in the deformed configuration it is necessary to match stress evaluations and strain specifications, that is the second Piola-Kirchhoff is coupled with Green-Lagrange strain and the Cauchy stress is matched with the infinitesimal strain [79]. This matching is sometimes referred to as energetically conjugated stress and strain [81].

The total Lagrangian formulation assumes the form [80]:

$$\begin{bmatrix} {}^{t}_{0}\mathbf{K}_{uu} & {}^{t}_{0}\mathbf{K}_{up} \\ {}^{t}_{0}\mathbf{K}_{pu} & {}^{t}_{0}\mathbf{K}_{pp} \end{bmatrix} \begin{Bmatrix} \overline{\mathbf{U}} \\ \overline{\mathbf{P}} \end{Bmatrix} = \begin{Bmatrix} {}^{t+\Delta t}\mathbf{R} \\ 0 \end{Bmatrix} - \begin{Bmatrix} {}^{t}_{0}\mathbf{F}_{u} \\ {}^{t}_{0}\mathbf{F}_{p} \end{Bmatrix}, \tag{42}$$

where $\overline{\mathbf{U}}$ and $\overline{\mathbf{P}}$ are respectively the increments in displacement and pressure relative to the reference configuration, ${}^{t+\Delta t}\mathbf{R}$ is the new externally applied vector load and ${}^{t}_{0}\mathbf{F}$ is the vector of nodal forces equivalent to the stress at time t. According to this notation [79], the left superscript indicates at which time the variable is being considered and the left subscript indicates the reference time with which measured changes are being evaluated. That said, it follows that the updated

Lagrangian formulation [41] is identical in form to the total Lagrangian formulation, except that the left subscript now changes from '0' to 't' [80].

The precise generation of $\mathbf{K}$ (and $\mathbf{F}$) using the total and updated Lagrangian formulations are well documented in the literature [68, 79]. For an analysis of a rubber material one should consult [41, 80]. Since the alternative analysis procedure of Sections 3.1 and 3.2 are based on utilisation of strain-energy functions W defined in Section 2 we will illustrate how the first element of $\mathbf{K}$, $\mathbf{K}_{uu}$, is determined using W for the simpler total Lagrangian formulation. The sub-matrix $\mathbf{K}_{uu}$ may in general be split into a linear and non-linear contribution, written as $\mathbf{K}_{uu} = \mathbf{K}_{uu}^{L} + \mathbf{K}_{uu}^{NL}$.

$\mathbf{K}_{uu}^{L}$ is dependent upon the fourth-order constitutive elastic tensor C_{ijhk} and $\mathbf{K}_{uu}^{NL}$ is a function of the second Piola-Kirchhoff stress tensor, S_{ij}. The stress and constitutive tensors in these cases are related to the strain-energy function W as follows:

$$ {}_0^t\overline{S}_{ij} = \frac{\partial {}_0^t\overline{W}}{\partial {}_0^t\varepsilon_{ij}} \quad \text{and} \quad {}_0^t\overline{C}_{ijhk} = \frac{\partial {}_0^t\overline{S}_{ij}}{\partial {}_0^t\varepsilon_{ij}} = \frac{\partial {}_0^t\overline{W}}{\partial {}_0^t\varepsilon_{ij}\partial {}_0^t\varepsilon_{hk}}, \tag{43} $$

where ε_{ij} are the components of the Green-Lagrange strain tensor and the over bar indicates that the quantity is not pressure dependent and only evaluated from displacement [80]. The Green-Lagrange strain tensor $\boldsymbol{\varepsilon}$ and the right Cauchy-Green deformation tensor $\mathbf{C}$ satisfy $\boldsymbol{\varepsilon} = \frac{1}{2}(\mathbf{C} - \mathbf{I})$. Introducing the notation: $\frac{\partial W(\mathbf{C})}{\partial \mathbf{C}} = \sum_{i=1}^{3} \frac{\partial W}{\partial \lambda_i^2}\frac{\partial \lambda_i^2}{\partial \mathbf{C}} = \sum_{i=1}^{3} \frac{\partial W}{\partial \lambda_i^2}\mathbf{N}_i \otimes \mathbf{N}_i$, where $\otimes$ is the tensor product or dyad, the second Piola-Kirchhoff stress tensor $\mathbf{S}$, of Equation (43), can be explicitly expressed in terms of the principal stretches $\lambda_i : i = 1, 2 \,\&\, 3$ as follows [82]:

$$ \mathbf{S} = 2\frac{\partial W}{\partial \mathbf{C}} \equiv \sum_{i=1}^{3} \frac{1}{\lambda_i}\frac{\partial W}{\partial \lambda_i}\mathbf{N}_i \otimes \mathbf{N}_i = \sum_{i=1}^{3} S_i \mathbf{N}_i \otimes \mathbf{N}_i \equiv \sum_{i=1}^{3} S_i \mathbf{N}_i \mathbf{N}_i^{\mathbf{T}}. \tag{44} $$

S_i is defined in Equation (11) and λ_i^2 & $\mathbf{N}_i$ are respectively the eigenvalues and eigenvectors of $\mathbf{C}$ defined in Section 2.1.

In the finite element analysis to be reported the updated Lagrangian formulation is used. However, corresponding details relating the strain-energy function to the finite element formulation are not given for the updated Lagrangian formulation, since their explanation is significantly more involved [41, 80], and there is only a need to indicate (in this paper) that the U/P formulation can be implemented through selection of any strain-energy function addressed by the selected software.

In the U/P formulation, irrespective of the Lagrangian formulation used, the displacement and the pressure are approximated with a summation over an appropriate shape function H_i. Formally:

$$u = \sum_{i=1}^{N} H_i^U u_i \text{ and } p = \sum_{i=1}^{N} H_i^P p_i \,, \tag{45}$$

where N represents the number of nodes defining each element used in the discretisation process and u_i, p_i represent the nodal value of displacement and pressure. For a reliable analysis the polynomial shape functions H_i^U & H_i^P should satisfy the Babuska-Brezzi (BB) condition [83] otherwise known as the Ladyzhenskaya-Babuska-Brezzi (LBB) condition [83] or the inf-sup condition [41, 83]. The derivation and implications of this mathematical condition are addressed in [83, 84]. The practical consequence of the inf-sup condition is that the displacement and pressure spaces cannot be chosen arbitrarily. A necessary, but not sufficient, condition to fulfil the inf-sup condition in the mixed method is the requirement that the pressure shape function must be of a lower order than the displacement shape function, i.e. $\dim\left(P^h\right) < \dim\left(U^h\right)$ where P^h and U^h are the associated spaces of pressure and displacement interpolation functions respectively.

In the FEA undertaken the selected solid elements are capable and appropriate to perform analyses involving large deformations [85]. The C3D8H hexahedral element is chosen for its simplicity. The C3D8H element is based on a linear interpolation for displacement and a constant value for the pressure. Whilst this element complies with the stated necessary condition, the difference in the dimensionality of the shape functions is not sufficient to satisfy the LBB condition. However, it is an effective and quite widely used element [41] as it: avoids locking problems [86]; it has been successfully applied in analysing the complex form of mitral valves [87]; and has been utilized in investigating aneurysms in blood vessels [88]. Furthermore, it is noted that C3D8H is a hybrid formulation of the continuum element C3D8 used in finite element simulations involving large displacements and deformations [89, 90]; hence it is deemed suitable for investigating the potentially large strain that may occur prior to the onset of the critical pressure. In the analysis to be reported [44] and in other cited papers the radial stretch parameter at critical pressure lies between 1.6 and 1.9, corresponding to 60% to 90% strain. For hyper-elastic material these are not large strains.

The higher order hexahedral element C3D20H provides quadratic interpolation for the displacement and linear interpolation for pressure. Comparisons of prediction based on C3D8H and C3D20H permits assessment of the effect of higher levels of interpolation within our analysis [44]. These two

solid elements are capable of providing the six zero-energy (rigid body) modes [see Table 1.2.1-10 of 91].

To exploit the cylindrical geometry of the distensible tubes investigated, yet another alternative axisymmetric quadrilateral element with hybrid interpolation is used, namely the CAX4H element with four nodes and its linear interpolation for the displacement and constant pressure. Again to assess the influence of a higher level of interpolation the eight nodes of the CAX8H are used to provide quadratic interpolation for the displacement and linear pressure.

In common with the previous elements the S4R shell element with reduced integration, is capable of large deformations [90] and generation of the six zero-energy modes [Table 1.2.1-6 of 91]. The S4R element has been used to provide: reference solutions for many benchmark problems for geometric nonlinear analysis [92]; biomedical aneurysm simulation [51]; and aneurysms in rubber material [23, 24].

It may be noted that the equivalence of U/P and reduced integration method has been established for limited applications by Malkus & Hughes [93]. According to Gadala [94] equivalence is not established for axisymmetric and three dimensional problems. Furthermore, Gadala quotes other sources as justification of the mixed (U/P) models over reduced/selective integration methods in geometric non-linear analysis. Comparison of the predictions (Section 4 and [44]) for the different selected elements cited may provide additional material for this discussion.

3.3.2 Finite element solution

The finite element analysis of an aneurysm has been formulated as a non-linear static problem. In general non-linear static problems may be solved using the classical Newton-Raphson method [41]. In this case direct application of Newton-Raphson is inappropriate because of the complex nature of the interactions of geometry, material properties, loads and boundary conditions. As the membrane load increases the positive stiffness reduces until at maximum load the stiffness becomes zero and critical pressure is attained. Beyond the critical pressure the structural stiffness is negative and further deformation is achieved with lower loads, hence near and beyond the point of critical pressure the Newton-Raphson approach cannot be used. Consequently a path following method such as the Riks algorithm [22] or existing modifications [95, 96] is necessary to investigate the

behaviour of a cylindrical hyper-elastic membrane subject to inflation. This method is now summarised.

Defining $v \in R^N$ as the unknown variable of N components the nonlinear static problem may be written as $F(v)=0$. A direct solution of this equation is not possible and the governing equation is recast in the form:

$$F(v,\lambda)=0,$$

where λ is the loading proportionality factor, or scaling factor for the external load. This parameter is introduced with the purpose of changing the load level during the iterative solution procedure, whereby the error associated with $F(v,\lambda)=0$ is reduced by forcing the solution to move along a particular curve (or straight line path) designated $f(v,\lambda)=0$. This approach may be captured by reformulating the problem in the form

$$G(w)=\begin{bmatrix} F(v,\lambda) \\ f(v,\lambda) \end{bmatrix} \text{ with } (w)=\begin{bmatrix} v \\ \lambda \end{bmatrix}.$$

The solution of the new system of equations is obtained with a prediction stage and a correction stage. The process starts from the initial undeformed situation $\lambda=0$ and the known solution v_0=0. The next step is to increment λ and v to obtain new values (v_1, λ_1) to satisfy $F(v,\lambda)=0$ iteratively. In a prediction stage a guess of the new equilibrium position is created and subsequently corrected using Newton-Raphson iterations $\left[v_1^{(1)}, v_1^{(2)}, ..., v_1^{(i)}\right]$ until the new equilibrium position v_1 is reached. Once the n=1 solution is found a sequence of solutions can be determined as illustrated in Figure 5.

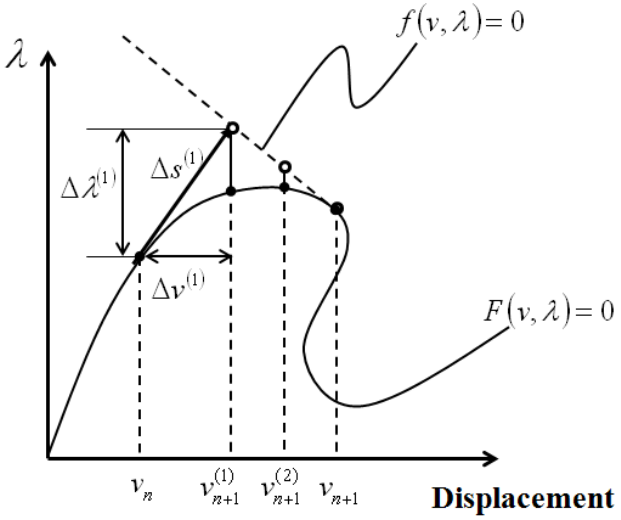

Fig. 5 Graphical illustration of Riks method for N=1 (based on [97])

The primitive variables in the Riks algorithm (readily available in most finite element packages) are simply displacement in a displacement based formulation or displacement and pressure in the U/P mixed formulation. Common to both approaches is inclusion of the load proportionality factor λ. This factor both influencing and being influenced by the incremental arc length steps taken along the equilibrium path *F* in the load-displacement plane. That is, arc length control is a combination of pure load control and pure displacement control. The Riks method permits development of the equilibrium path up to and beyond the limit point represented by the critical pressure.

The veracity of the generated equilibrium path beyond the critical pressure point depends upon whether alternative branches exist. Mathematically the existence of alternative paths is referred to as bifurcation of the solution. Assessing whether or not bifurcation has occurred requires an investigation of the positive definiteness of the associated tangent stiffness matrix $\mathbf{K}_T$. This can be measured by looking at the smallest pivot or the determinant of indicated stiffness matrix or its lowest eigenvalue [98]. Computationally the more efficient approach is the study of the diagonal members of the $\mathbf{L}$ matrix in the $\mathbf{LU}$ decomposition of the tangent stiffness matrix $\mathbf{K}_T = \mathbf{LU}$. The value of all diagonal elements of the upper triangular matrix $\mathbf{U}$ is unity. A sufficient condition for instability (bifurcation) is the existence of a negative diagonal element L_{ii} [99]. During application of the Riks arc-length method the likelihood that one of the solution points (defining the arc) correspond to a singular point is remote. Therefore, since the diagonal elements of $\mathbf{L}$ are continuous functions of the path parameters, the existence of singular points between two adjacent computation points can be readily determined by monitoring sign changes of the diagonal elements L_{ii} [99]. In the ABAQUS® software this option is implemented in the sense that warnings are issued regarding behaviour of the eigenvalues.

Bifurcation arises when a structure and loading system are without any imperfections, such as those attributable to manufacturing, assembling et cetera [98]. The presence of many bifurcation points is found after the achievement of the maximum pressure [14, 100, 101, 102], or, in the neighbourhood of the critical pressure with the first bifurcation point before the critical pressure [21, 103]. These bifurcation points tend to cluster together when the tube becomes longer [14, 21] with higher values of the aspect ratio $2l_0/r_0$. Haughton & Ogden [103] found two theoretically possible bifurcation modes in their investigation of a cylindrical hyper-elastic tube. In one mode the cylindrical membrane remains prismatic with non circular cross-section. In the other mode the tube experiences the formation of an axisymmetric bulge whilst the cross-sections remain circular. For each case to

exist certain mathematical conditions were derived. However, Haughton & Ogden deemed the mathematical conditions required for the prismatic non-circular cross-section were physically impossible in a real elastic material.

Once the existence of bifurcation has been established, the introduction of a perturbation removes the bifurcation and solution of the slightly modified problem provides the branch most sensitive to the perturbation introduced. In finite element analysis this may be achieved by perturbing either the geometry through the addition of weighted buckling eigenmodes [21, 46, 98], or, the load. Shi & Moita [21] in their post-critical analysis of an inflated cylindrical membrane suggested that the clamped boundary condition could be seen as a perturbation of the perfect geometry.

In the reported analyses of Section 4, and the companion paper [44], no buckling eigenmode is introduced as a perturbation of the initial perfect geometry. Under this condition the ABAQUS® software predicts a post-buckling behaviour of a cylindrical membrane consistent with the first symmetric bifurcation mode, that is, a bulge deformation symmetric with respect to the tube mid-span. In just a few cases [44] a higher bifurcation mode persists with symmetric bulge-like deformations located either side of the tube mid-span. According to Shi & Moita [21] the first bifurcation mode is the most likely mode to occur because it is associated with the lowest deformation energy.

In this paper the authors are primarily concerned with the occurrence of critical pressure and not a complete post-critical (post-buckling) analysis.

4. Presentation and discussion of representative results

Representative results are presented for each of the three analysis methods described, subject to application of some or all the strain-energy functions and complete sets of experimental data based on Treloar or Treloar and Kawabata et al. The companion paper [44] provides an in-depth investigation using different combinations of data sets provided by Treloar and Kawabata et al., application of the strain-energy functions defined in Sections 2.2.2 and the three alternative analysis procedures. Only the finite element method can readily adopt the Marlow strain-energy function approach, see Section 2.2.3.

4.1 Critical and propagation pressure for a long thin-walled tube

The first representative results address critical pressure prediction using the simplified analysis based on Equations (24), (26b) and (28) for tube radius $r_0 = 0.01$m and initial thickness $t_{w0} =$ 0.001m. As each possible strain-energy function is selected Equations (28) are transformed to those presented in Equations (29). Using the Treloar uniaxial, equi-biaxial and pure shear data we find that the pressure variation with circumferential stretch (λ_1) is quite distinct depending upon the strain-energy functions selected. In Figure 6a the Neo-Hookean, Mooney-Rivlin and Ogden (N=1) strain-energy functions lead to monotonically decreasing pressure beyond the critical pressure. In contrast Figure 6b indicates that the Yeoh, Arruda-Boyce and Ogden (N=2 & N=3) models exhibit the 'N' shape pressure variation expected from experimental observations of inflated tubes [12, 13, 14, 30]. The value of λ_1 associated with the critical pressure is very similar magnitude for all models apart from Ogden (N=2), with corresponding critical pressures in the range 28.0 to 31.5kPa. Arruda-Boyce predicts a rather low critical pressure of 25.6kPa.

The distinct characteristic differences in the pressure variation, beyond critical pressure, in Figures 6a & b have implications beyond that of simply reflecting changes due to selection of a different strain-energy function of vary complexity.

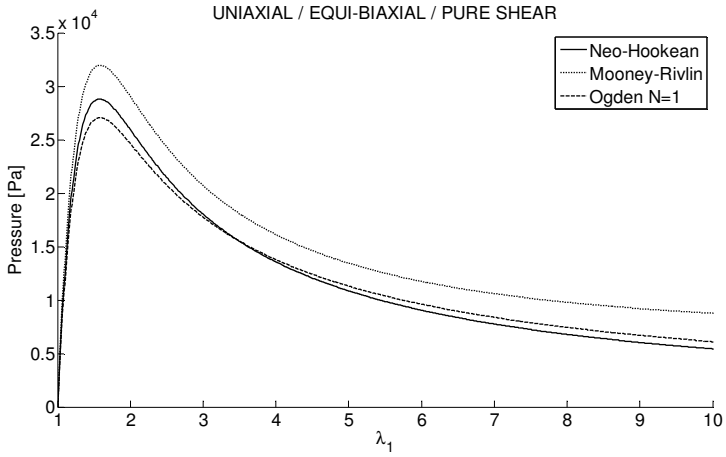

Fig. 6a. $P - \lambda_1$ **curves with only maximum pressure (Treloar rubber)**

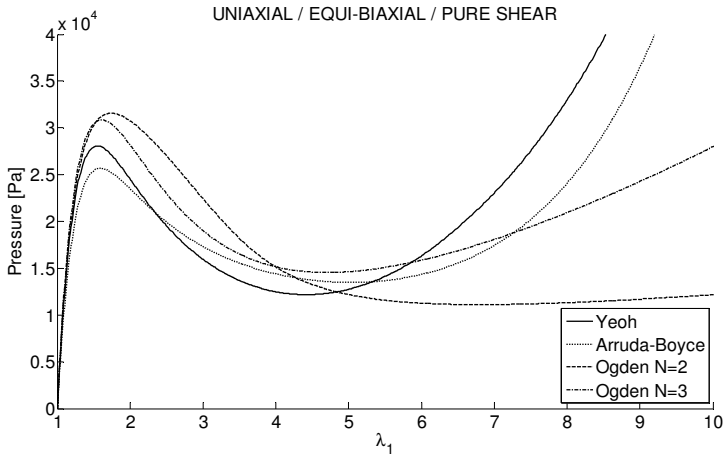

Fig. 6b. $P-\lambda_1$ **curves with maximum and minimum pressure (Treloar rubber)**

Mathematically the pressure may continue to reduce monotonically beyond its peak value, or, it may decrease to a minimum and then rise for further increases in the stretch parameter λ_1. These two possible outcomes, clearly indicated in Figures 6, have quite distinct implications. In the first case (Figure 6a) the non existence of a minimum pressure implies that aneurysm propagation is not feasible according to the Maxwell equal area rule [13, 16, 30]; the second case (Figure 6b) associated with a longitudinal aneurysm propagation is consistent with experimental observation [12, 13, 14, 30]. In short certain available strain-energy functions provide characteristics contrary to practical expectations. For this particular analysis procedure it readily follows that the rate of increase in volume relative to initial volume v_0, that is $V = v/v_0$, as pressure changes is proportional to $\lambda_1^2\lambda_2$ [15]. For the selected strain-energy functions the corresponding $P-V$ curves are presented in Figures 6c & d.

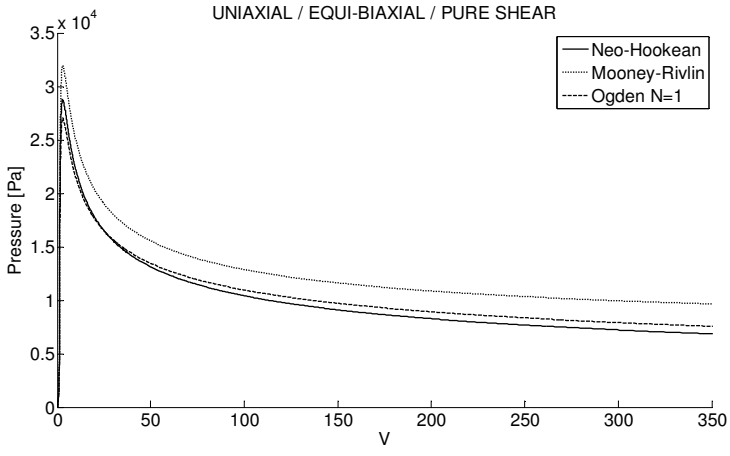

Fig. 6c. $P-V$ **curves with only maximum pressure (Treloar rubber)**

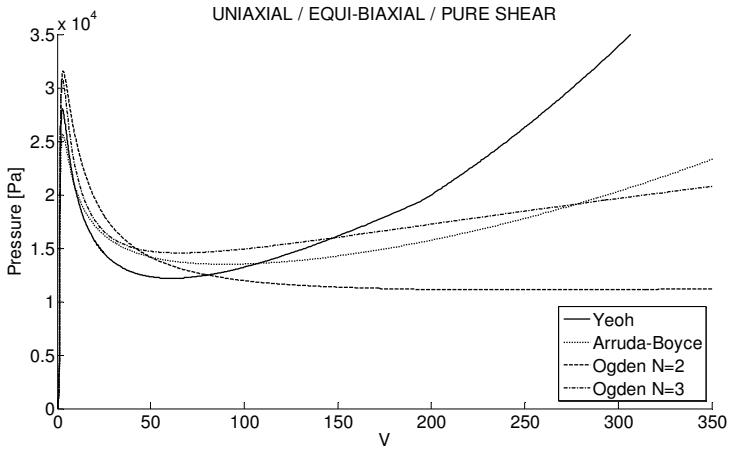

Fig. 6d. $P-V$ **curves with maximum and minimum pressure (Treloar rubber)**

Propagation pressure, P_p, is evaluated by determining the inflation pressure P such that Area A, under the $P-V$ curve and above the line $P = P_p$, equals Area B between the $P-V$ curve and below the line $P = P_p$, as illustrated in Figure 7.

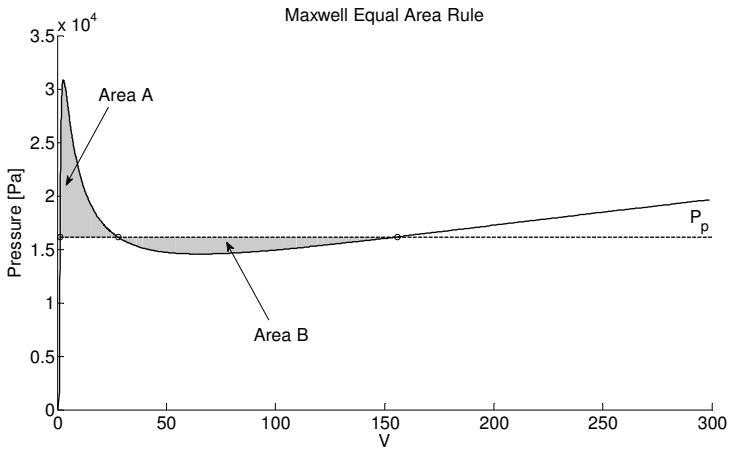

Fig. 7. Illustration of Maxwell equal area rule.

Replacing the full sets of Treloar data ([27] and Appendix A) with the corresponding full sets of Kawabata et al. data [31] the range of critical pressure values in Figures 8a & b are now smaller. We note that Yeoh strongly follows and Ogden (N=3) more weakly follows the expected 'N' shape in Figure 8b. Furthermore Neo-Hookean and Arruda-Boyce give essentially the same behaviour irrespective of the data sets used [44], i.e. any differences observed are very insignificant. For both sets of data critical pressure is associated with a λ_1-value in the interval 1.6–1.9.

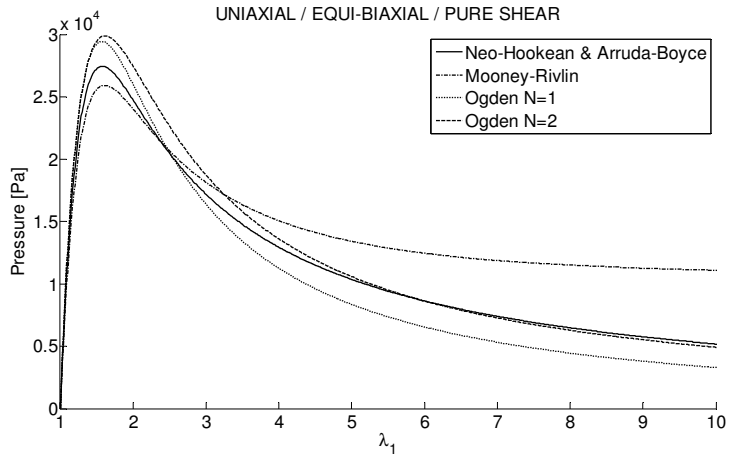

Fig. 8a. $P-\lambda_1$ **curves with only maximum pressure (Kawabata et al. rubber)**

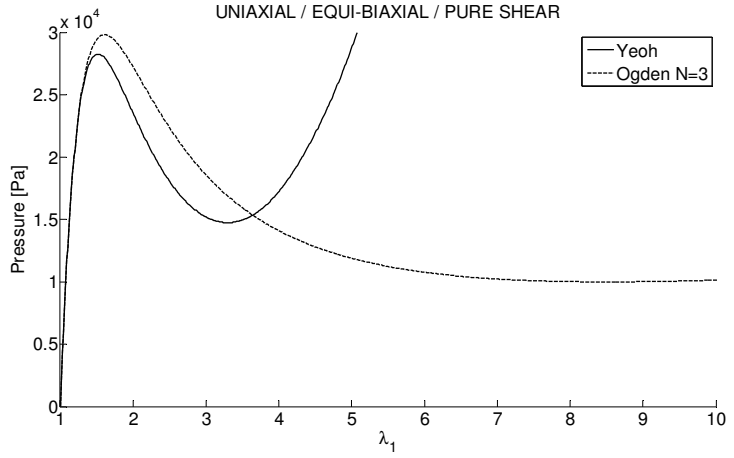

Fig. 8b. $P-\lambda_1$ **curves with maximum and minimum pressure (Kawabata et al. rubber)**

Figures 8c & d provide the corresponding Kawabata et al. data based $P-V$ curves.

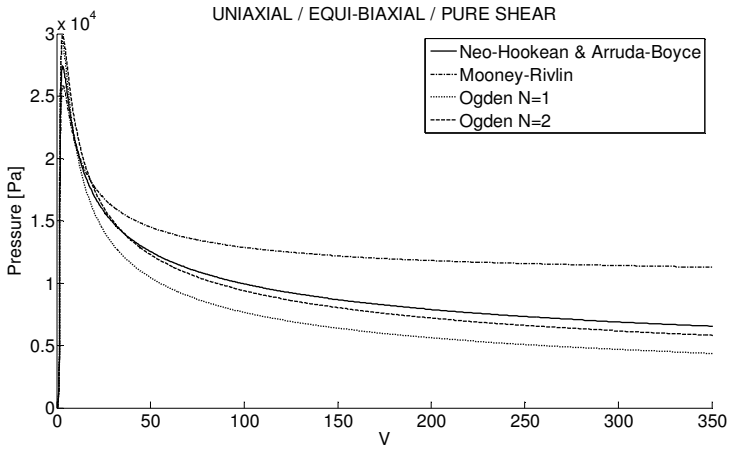

Fig. 8c. $P-V$ **curves with only maximum pressure (Kawabata et al. rubber)**

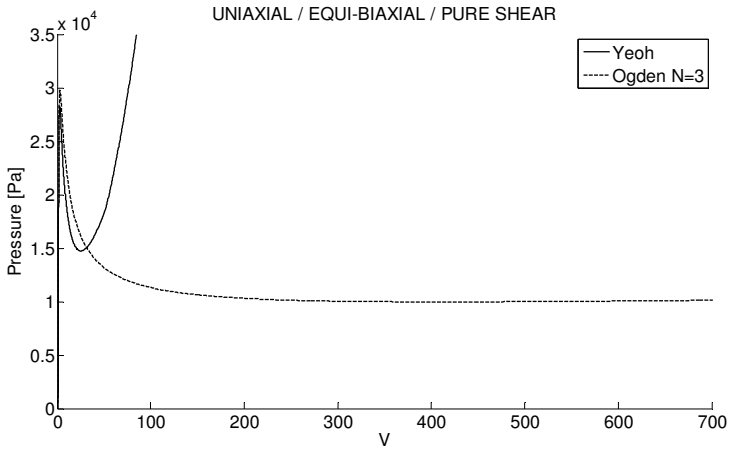

Fig. 8d. $P-V$ **curves with maximum and minimum pressure (Kawabata et al. rubber)**

The Treloar (Figure 6) and Kawabata et al. (Figure 8) based $P-\lambda_1$ curves have essentially the same behaviour and location of critical pressure. The Arruda-Boyce and Ogden (N=2) strain-energy functions are more acceptable in terms of the existence of minimum pressure when using a Treloar rather than a Kawabata based material. When a 'N' shape is obtained, calculation of the propagation pressure is possible. For the $P-V$ curves of Figures 6d & 8d, propagation pressure values are provided in Table 2.

Table 2 Propagation pressure

Propagation Pressure [Pa]	Model	Data source
12092.11	Ogden N = 2	Treloar [Appendix A]
16149.09	Ogden N = 3	
14222.22	Yeoh	
14866.65	Arruda-Boyce	
10638.28	Ogden N = 3	Kawabata et al. [31]
17268.27	Yeoh	

Clearly both the critical pressure and propagation pressure value are highly sensitive to the strain-energy function selected. For the Treloar material a small difference (around 0.7kPa) in the value of the critical pressure for Ogden N=2 and Ogden N=3 leads to a 4kPa difference for the propagation pressure. This behaviour is confirmed for the Kawabata material. In this case a 6.5kPa difference in P_p arises for a difference of 1.5kPa in critical pressure. This means the strain-energy functions are capturing a different critical pressure value and overall behaviour during inflation. The influence of end conditions for a tube of finite length are addressed next with predictions provided from solution of Equations (38).

4.2 Critical pressure results for an axisymmetric membrane long thin-walled tube

Sample results are now presented for an axisymmetric finite membrane with a length to radius ratio of $2l_0/r_0$ =10, an initial uniform radius of $r_0 = 0.01$m and a thickness of $t_{w0} = 0.001$m. The predictions presented are restricted to use of the three full sets of Treloar data. Figures 9a & b illustrate application of Equations (38) with the Yeoh and Ogden (N=3) strain-energy functions respectively; required strain-energy function derivatives are provided in Appendix B. Unlike the simpler approach the axisymmetric membrane model permits provision of the longitudinal variation of cross-section with changing λ_1. The required 'N' shape curve is also captured by this method. Comparison of Figure 6b with Figure 9a (for Yeoh) and Figure 9b (for Ogden N=3), indicates that critical pressure has comparable magnitude for corresponding λ_1-values. This method reflects the influence of a finite length of tube, giving a more realistic simulation. More in depth studies based on different data sets and other strain-energy function are reported in the companion paper [44].

Figures 9a & b indicate that Yeoh model has a steeper recovery than the Ogden model from the minimum pressure. Whilst this is in accordance with previous results illustrated in Figure 6b, further inspection is necessary to ascertain the benefit, or otherwise, of this observation.

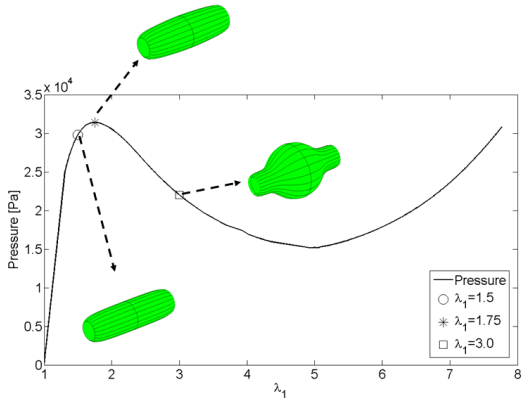

Fig. 9a. $P-\lambda_1$ **curves derived from shooting method with Yeoh and** $2l_0/r_0 = 10$

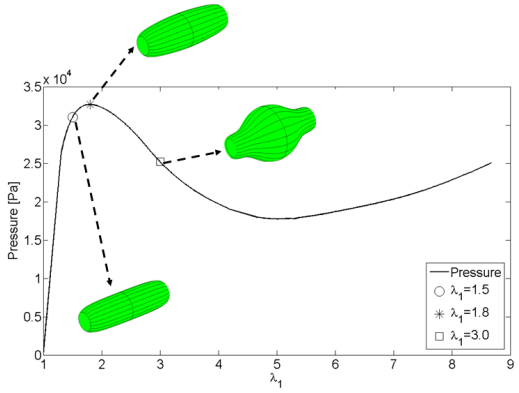

Fig. 9b. $P-\lambda_1$ **curves derived from shooting method with Ogden N=3 and** $2l_0/r_0 = 10$

The implicit end conditions within the axisymmetric membrane model is the invariance of the cross-section of the tube ends. Hence the end points maintain a radius of r_0 irrespective of assigned λ_1-values. Figures 9a & b illustrate the change in profile of the plane curve revolved to generate the axisymmetric tube for distinct λ_1-values. Figures 9c & e indicate how the membrane shape varies with λ_1 using the Yeoh and Ogden strain-energy function. Figures 9d & f provide magnified views of the membrane shape at the right-hand end of the tube. These magnified plots indicate, that for $\lambda_1 \in (1.31, 2.11)$ for Yeoh and $\lambda_1 \in (1.31, 2.51)$ for Ogden there is no effective tube elongation beyond the fixed end point. For higher λ_1-values the tube is stretched beyond the end point and the curvature is reversed to accommodate membrane equilibrium. Furthermore, in Figure 9d for $\lambda_1 = 3.70$ there is a rogue solution. This is not without precedence in the 'shooting' technique based approach. With appropriate effort one can force a preferred solution consistent with the other predictions. However, it is the critical pressure that is of primary interest here. Clearly a detailed examination of generated solutions is necessary to appreciate limitation of analysis procedure.

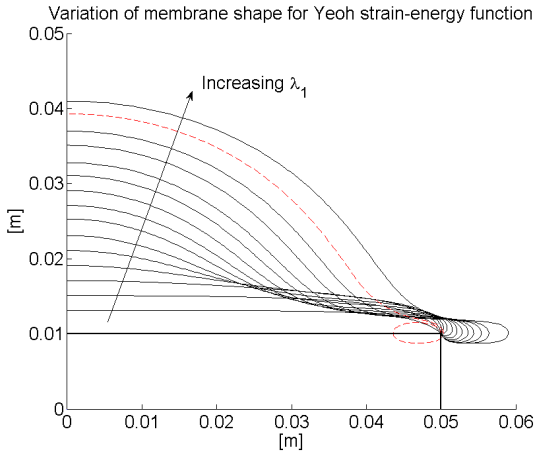

Fig. 9c. Variation of membrane shape for Yeoh model

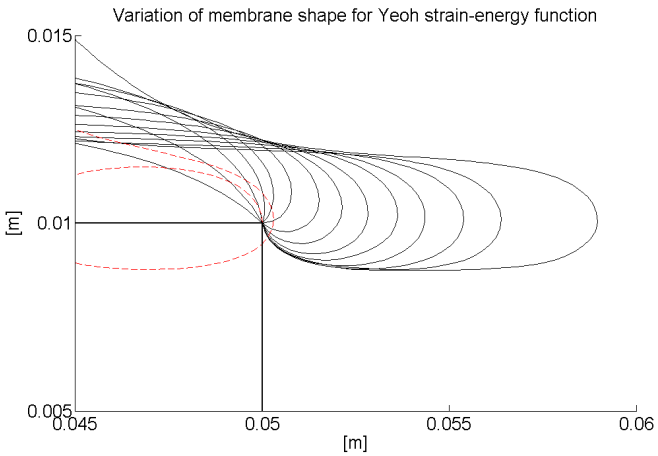

Fig. 9d. Magnified variation of membrane shape for Yeoh model

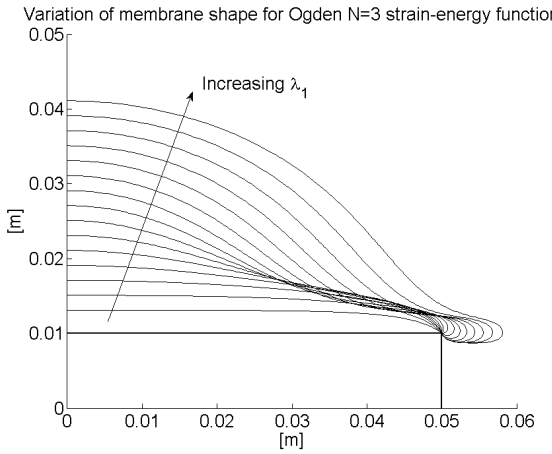

Fig. 9e. Variation of membrane shape for Ogden N=3 model

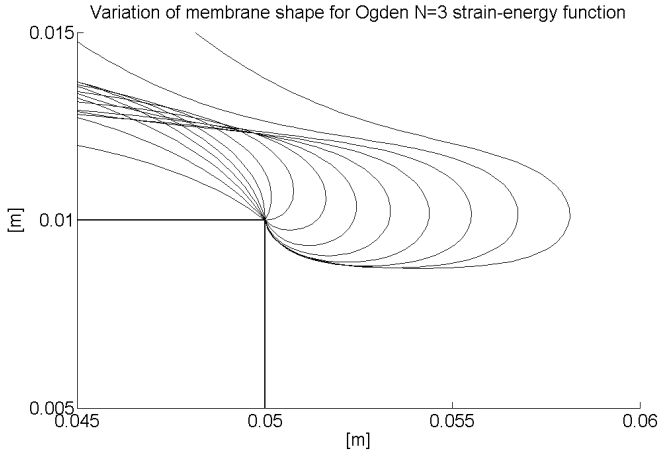

Fig. 9f. Magnified variation of membrane shape for Ogden N=3 model

Just as the application of the axisymmetric membrane represented a less constrained model than the long thin-walled tube so we now seek to remove further limitations through the application of the finite element approach.

4.3 Critical pressure results for finite element

For the same tube Figures 10 & 11 indicate the influence of different end conditions upon the shape of the FEA determined $P-\lambda_1$ curves. In this simulation the linear reduced integration shell S4R is used. The longitudinal variation of tube cross-section for corresponding λ_1-values is very similar in Figures 9, 10 & 11 for $\lambda_1 \le 3$. For larger values of λ_1 the shape comparison is meaningless due a fundamental difference in the axisymmetric membrane approach and the finite element method. In the analysis of Section 4.2 the stretch ratio λ_1 is imposed at the centre of the tube prior to solving

the governing equations using the appropriate λ_2^* - and P^* -values required to ensure satisfaction of Equation (37b). In the finite element analysis undertaken λ_1 is retrieved during the solution and is not assigned incrementally a priori. Consequently the 'shooting' method will attempt a solution for any assigned λ_1-value irrespective of whether the stretch ratio λ_1 is physically realistic in terms of the tube end deformations, as illustrated in Figures 9d & f.

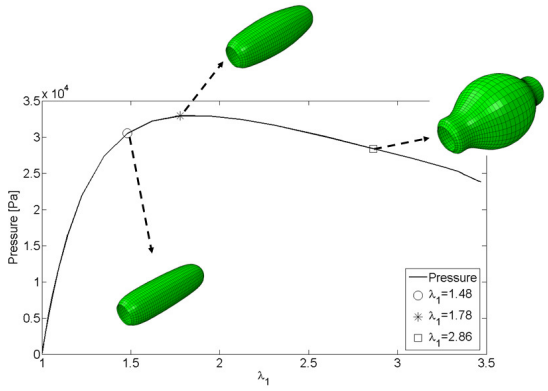

Fig. 10. $P-\lambda_1$ **curves derived from clamped-clamped FEA with Ogden N=3 and** $2l_0/r_0=10$

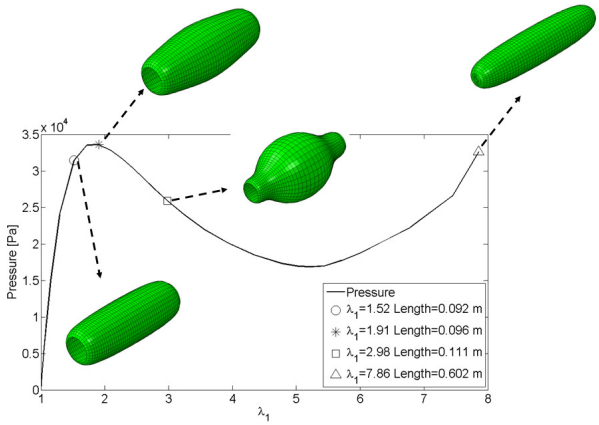

Fig. 11. $P-\lambda_1$ **curves derived from clamped-rolled FEA with Ogden N=3 and** $2l_0/r_0=10$

In Figure 10 a λ_1-value greater than 3.5 is not presented. Whereas in the previous membrane analysis we highlighted end tube distortion, in the finite element analysis one observes distortion in the tube at the starting (end) position of the bulbous aneurysm. In this region the deformation of the tube leads to a convergence problem. One might be tempted to assume that this finite element difficulty, in common with the application of the membrane method, is a consequence of preventing the tube naturally extending. The clamped boundary conditions applied at both ends may be relaxed with the introduction of the rolled condition at one end, that is, no radial translation occurs but this end may move longitudinally and rotate. Clearly in Figure 11 the rolled boundary condition at one tube end permits the elongation of the tube and removal of cited numerical challenges. The truncation of the λ_1 range in Figure 11 does not imply any limitation.

5. Conclusions

Three different approaches are reviewed for the prediction of critical pressure.

The first method presented captures the essential physics of the aneurysm development and constitutes a fast tool readily implemented. The predicted critical pressures are of sufficient accuracy for appreciating the likelihood of an aneurysm. Furthermore, it can be used to provide initial estimates of parameters for the more refined and general axisymmetric membrane model.

The membrane model method is more difficult to implement and requires finer numerical tuning to successfully obtain converged results. This approach permits prediction of the membrane shape and, as will be demonstrated in the companion paper, provides predictions in close agreement with the finite element analysis.

Having failed to locate a research paper containing derivation of governing equations for an axisymmetric membrane the equations have been derived here from first principle for completeness.

The finite element provides greater analysis scope through greater choice of element selection, boundary conditions imposed and material modelling. Furthermore, it constitutes a tool equally available to academic and industrial researchers active in different fields of engineering, hydrodynamics and bio-medical sciences.

All generated predictions demonstrate the sensitivity of critical pressure to selected strain-energy function. This is also true for the propagation pressure predictions.

An appropriate test of whether a strain-energy function is suitable for investigated initiation and propagation of an aneurysm is the Maxwell equal area requirement.

For the Treloar and Kawabata data it appears that the required ‘N’ shape variation of inflation pressure with radial stretch ratio is correctly provided by the Yeoh and third-order Ogden strain-energy function.

The variation of critical pressure with respect to the selection of different experimental data sets for each strain-energy function will be addressed in depth in the companion paper. Direct numerical comparisons of predictions based on the three different techniques presented in this paper will be provided with discussion and critical review.

Appendix A

Table A1 Treloar retrieved data

Uniaxial		Equi-biaxial		Pure Shear	
Stress [Pa]	Strain	Stress [Pa]	Strain	Stress [Pa]	Strain
140110	0.144	92057.04	0.02	72176.5845	0.03802
230196	0.247	155979.00	0.06	167213.412	0.12388
320368	0.410	236293.47	0.11	250829.928	0.19062
410600	0.615	257218.20	0.14	338332.185	0.3053
500946	0.901	326084.40	0.20	422092.908	0.44878
581299	1.186	434367.18	0.31	593629.587	0.85081
671589	1.431	508452.30	0.42	765421.326	1.38715
852311	2.023	647695.44	0.68	941098.806	1.97142
1052996	2.595	763159.14	0.94	1124206.38	2.46932
1223493	3.024	959977.17	1.49	1288308.06	2.95773
1594292	3.761	1239503.31	2.03	1467438.66	3.35973
1954917	4.375	1440147.24	2.43	1627449.57	3.68509
2305242	4.765	1706940.00	2.75	1802518.83	3.95282
2695562	5.176	1972378.98	3.07		
3045652	5.404	2202364.62	3.26		
3415724	5.631	2418459.30	3.45		
3775830	5.879				
4145853	6.066				
4495766	6.172				
4875658	6.277				
5235646	6.444				
5595496	6.509				

In the original Treloar paper [27] equi-biaxial data is provided in tabulated form. The uniaxial and pure shear data is presented graphically. To convert the Treloar raw equi-biaxial data (column 5 of Table I [27]) to SI units of nominal stress the data are weighted by $g \cdot \lambda \cdot 10^4$. The Treloar graphical data (Figure 3 [27] for uniaxial and Figure 7 [27] for pure shear) are converted to SI units for nominal stress by weighting graphical readings by $g \cdot 10^4$.

Appendix B

The pure and mixed derivatives of the strain-energy function with respect to λ_1 and λ_2 are presented here since they are required for the axisymmetric membrane model of Section 3.2.

Mooney-Rivlin

$$\frac{\partial \hat{W}}{\partial \lambda_1} = C_{10}\left[2\lambda_1 - \frac{2}{\lambda_1^3\lambda_2^2}\right] + C_{01}\left[-\frac{2}{\lambda_1^{\,3}} + 2\lambda_1\lambda_2^2\right] \qquad \frac{\partial \hat{W}}{\partial \lambda_2} = C_{10}\left[2\lambda_2 - \frac{2}{\lambda_1^2\lambda_2^3}\right] + C_{01}\left[-\frac{2}{\lambda_2^{\,3}} + 2\lambda_1^2\lambda_2\right]$$

$$\frac{\partial^2 \hat{W}}{\partial \lambda_1^2} = C_{10}\left[2 + \frac{6}{\lambda_1^4\lambda_2^2}\right] + C_{01}\left[\frac{6}{\lambda_1^4} + 2\lambda_2^2\right] \qquad \frac{\partial^2 \hat{W}}{\partial \lambda_1 \partial \lambda_2} = C_{10}\left[\frac{4}{\lambda_1^3\lambda_2^3}\right] + C_{01}\left[4\lambda_1\lambda_2\right]$$

Ogden

$$\frac{\partial \hat{W}}{\partial \lambda_1} = \sum_{i=1}^{N}\mu_i\left[\lambda_1^{\alpha_i-1} - \frac{1}{\lambda_1^{\alpha_i+1}\lambda_2^{\alpha_i}}\right] \qquad \frac{\partial \hat{W}}{\partial \lambda_2} = \sum_{i=1}^{N}\mu_i\left[\lambda_2^{\alpha_i-1} - \frac{1}{\lambda_1^{\alpha_i}\lambda_2^{\alpha_i+1}}\right]$$

$$\frac{\partial^2 \hat{W}}{\partial \lambda_1^2} = \sum_{i=1}^{N}\mu_i\left[(\alpha_i-1)\lambda_1^{\alpha_i-2} + \frac{(\alpha_i+1)}{\lambda_1^{\alpha_i+2}\lambda_2^{\alpha_i}}\right] \qquad \frac{\partial^2 \hat{W}}{\partial \lambda_1 \partial \lambda_2} = \sum_{i=1}^{N}\mu_i\left[\frac{\alpha_i}{\lambda_1^{\alpha_i+1}\lambda_2^{\alpha_i+1}}\right]$$

Neo-Hookean

$$\frac{\partial \hat{W}}{\partial \lambda_1} = C_{10}\left[2\lambda_1 - \frac{2}{\lambda_1^3\lambda_2^2}\right] \qquad \frac{\partial \hat{W}}{\partial \lambda_2} = C_{10}\left[2\lambda_2 - \frac{2}{\lambda_1^2\lambda_2^3}\right]$$

$$\frac{\partial^2 \hat{W}}{\partial \lambda_1^2} = C_{10}\left[2 + \frac{6}{\lambda_1^4\lambda_2^2}\right] \qquad \frac{\partial^2 \hat{W}}{\partial \lambda_1 \partial \lambda_2} = C_{10}\left[\frac{4}{\lambda_1^3\lambda_2^3}\right]$$

Yeoh

$$\frac{\partial \hat{W}}{\partial \lambda_1} = \left[C_{10} + 2C_{20}(I_1-3) + 3C_{30}(I_1-3)^2\right]\left[2\lambda_1 - \frac{2}{\lambda_1^3\lambda_2^2}\right]$$

$$\frac{\partial \hat{W}}{\partial \lambda_2} = \left[C_{10} + 2C_{20}(I_1-3) + 3C_{30}(I_1-3)^2\right]\left[2\lambda_2 - \frac{2}{\lambda_1^2\lambda_2^3}\right]$$

$$\frac{\partial^2 \hat{W}}{\partial \lambda_1^2} = \left[2C_{20} + 6C_{30}(I_1-3)\right]\left(2\lambda_1 - \frac{2}{\lambda_1^3\lambda_2^2}\right)^2 + \left[C_{10} + 2C_{20}(I_1-3) + 3C_{30}(I_1-3)^2\right]\left[2 + \frac{6}{\lambda_1^4\lambda_2^2}\right]$$

$$\frac{\partial^2 \hat{W}}{\partial \lambda_1 \partial \lambda_2} = \left[2C_{20} + 6C_{30}(I_1-3)\right]\left[2\lambda_1 - \frac{2}{\lambda_1^3\lambda_2^2}\right]\left[2\lambda_2 - \frac{2}{\lambda_1^2\lambda_2^3}\right] + \left[C_{10} + 2C_{20}(I_1-3) + 3C_{30}(I_1-3)^2\right]\left[\frac{4}{\lambda_1^3\lambda_2^3}\right]$$

Arruda-Boyce

$$\frac{\partial \hat{W}}{\partial \lambda_1} = \mu\left(2\lambda_1 - \frac{2}{\lambda_1^3\lambda_2^2}\right)\sum_{i=1}^{5} i\frac{C_i}{\lambda_m^{2i-2}}\left(I_1^{i-1}\right)$$

$$\frac{\partial \hat{W}}{\partial \lambda_2} = \mu\left(2\lambda_2 - \frac{2}{\lambda_1^2\lambda_2^3}\right)\sum_{i=1}^{5} i\frac{C_i}{\lambda_m^{2i-2}}\left(I_1^{i-1}\right)$$

$$\frac{\partial^2 \hat{W}}{\partial \lambda_1^2} = \mu\left(2 + \frac{6}{\lambda_1^4\lambda_2^2}\right)\sum_{i=1}^{5} i\frac{C_i}{\lambda_m^{2i-2}}\left(I_1^{i-1}\right) + \mu\left(2\lambda_1 - \frac{2}{\lambda_1^3\lambda_2^2}\right)^2\sum_{i=2}^{5}\left(i^2 - i\right)\frac{C_i}{\lambda_m^{2i-2}}\left(I_1^{i-2}\right)$$

$$\frac{\partial^2 \hat{W}}{\partial \lambda_1 \partial \lambda_2} = \mu\left(\frac{4}{\lambda_1^3\lambda_2^3}\right)\sum_{i=1}^{5} i\frac{C_i}{\lambda_m^{2i-2}}\left(I_1^{i-1}\right) + \mu\left(2\lambda_1 - \frac{2}{\lambda_1^3\lambda_2^2}\right)^2\sum_{i=2}^{5}\left(i^2 - i\right)\frac{C_i}{\lambda_m^{2i-2}}\left(I_1^{i-2}\right)$$

References

[1] W.A. Osborne, W. Sutherland, The Elasticity of Rubber Balloons and Hollow Viscera, Proceedings of the Royal Society of London – Part B – Biological Sciences, 81 (1909) 485–499.

[2] I. Müller, H. Struchtrup, Inflating a Rubber Balloon, Mathematics and Mechanics of Solids, 7 (2002) 569–577.

[3] D.A. Vorp, Biomechanics of abdominal aortic aneurysm (Review), Journal of Biomechanics, 40 (2007) 1887–1902.

[4] M.L. Raghavan, M.M. Hanaoka, J.A. Kratzberg, M. de Lourdes Higuchi, E.S. da Silva, Biomechanical failure properties and microstructural content of ruptured and unruptured abdominal aortic aneurysm, Journal of Biomechanics, 44 (2011) 2501–2507.

[5] R.S. Mitchell, M.D. Dake, C.P. Semba, T.J. Fogarty, C.K. Zarins, R.P. Liddell, D.C. Miller, Endovascular stent-graft repair of thoracic aortic aneurysms, The Journal of Thoracic and Cardiovascular Surgery, 111 (1996) 1054–1062.

[6] A.N. Gent, Elastic instabilities in rubber – Aneurysms, wrinkles and knots, in: J.J.C. Busfield, A.H. Muhr (Eds.), Constitutive Models for Rubber III, Taylor & Francis, 2003, pp. 95–98.

[7] A.N. Gent, Elastic instabilities in rubber, International Journal of Non–Linear Mechanics, 40 (2005) 165–175.

[8] A. Mallock, Note on the Instability of India–Rubber Tubes and Balloons When Distended by Fluid Pressure, Proceedings of the Royal Society of London, 49 (1890–1891) 458–463.

[9] H. Alexander, Tensile instability of initially spherical balloons, International Journal of Engineering Sciences, 9 (1971) 151–162.

[10] A. Needleman, Inflation of spherical rubber balloons, International Journal of Solids and Structures, 13 (1977) 409–421.

[11] D.M. Haughton, Post-bifurcation of Perfect and Imperfect Spherical Elastic Membranes, International Journal of Solids and Structures, 16 (1980) 1123–1133.
[12] H. Alexander, The tensile instability of an inflated cylindrical membrane as affected by an axial load, International Journal of Mechanical Sciences, 13 (1971) 87–95.
[13] S. Kyriakides, Y.C. Chang, On the inflation of a long elastic tube in the presence of axial load, International Journal of Solids and Structures, 26 (1990) 975–991.
[14] S. Kyriakides, Y.C. Chang, The initiation and propagation of a localized instability in an inflated elastic tube, International Journal of Solids and Structures, 27 (1991) 1085–1111.
[15] L.M. Kanner, C.O. Horgan, Elastic instabilities for strain-stiffening rubber-like spherical and cylindrical thin shells under inflation, International Journal of Non-Linear Mechanics, 42 (2007) 204–215.
[16] Y.B. Fu, S.P. Pearce, K.K. Liu, Post-bifurcation analysis of a thin-walled hyperelastic tube under inflation, International Journal of Non-linear Mechanics, 43 (2008) 697–706.
[17] X. Guo, Kinematic modeling of finite axisymmetric inflation for an arbitrary polymeric membrane of revolution, Polymer-Plastics Technology and Engineering, 40 (3) (2001) 341–361.
[18] X. Guo, Large deformation analysis for a cylindrical hyperelastic membrane of rubber-like material under internal pressure, Rubber Chemistry and Technology, 74 (2001) 100–115.
[19] W. Cheney, D. Kincaid, Numerical Mathematics and Computing, sixth ed., Thomson Brooks/Cole, Belmont (CA), 2007.
[20] W.H. Yang, W.W. Feng, On Axisymmetrical Deformations of Nonlinear Membranes, Journal of Applied Mechanics, 37 (1970) 1002–1011.
[21] J. Shi, G.F. Moita, The post-critical analysis of axisymmetric hyper-elastic membranes by the finite element method, Computer Methods in Applied Mechanics and Engineering, 135 (1996) 265–281.
[22] E. Riks, An Incremental Approach to the Solution of Snapping and Buckling Problems, International Journal of Solids and Structures, 15 (1979) 529–551.
[23] D. Pamplona, P.B. Goncalves, S.R.X. Lopes, Finite deformations of cylindrical membrane under internal pressure, International Journal of Mechanical Sciences, 48 (2006) 683–696.
[24] P.B. Goncalves, D. Pamplona, S.R.X. Lopes, Finite deformations of an initially stressed cylindrical shell under internal pressure, International Journal of Mechanical Sciences, 50 (2008) 92–103.
[25] S.R. Xavier, Comportamento Não-Linear e Instabilidade de Membranas e Cascas Hiperelasticas, PhD dissertation, Civil Engineering Department, Pontificial Catholic University, PUC-Rio, Rio de Janeiro, Brazil (2003), (in Portuguese).

[26] British Standard, BS 903-5, Physical testing of rubber – Part 5: Guide to the application of rubber testing to finite element analysis, (2004) 1 – 43.
[27] L.R.G. Treloar, Stress–strain data for vulcanised rubber under various types of deformation, Transactions of the Faraday Society, 40 (1944) 59–70.
[28] R.W. Ogden, Large deformation isotropic elasticity – on the correlation of theory and experiment for incompressible rubber-like solids, Proceedings of the Royal Society of London, 326 (1972) 565–584.
[29] R.W. Ogden, Nonlinear Elastic Deformations, Dover Publications, Mineola (N.Y), 1997.
[30] E. Chater, J.W. Hutchinson, On the propagation of bulges and buckles, Journal of Applied Mechanics, 51 (1984) 269–277.
[31] S. Kawabata, M. Matsuda, K. Tei, H. Kawai, Experimental Survey of the Strain Energy Density Function of Isoprene Rubber Vulcanizate, Macromolecules, 14 (1981) 154–162.
[32] L.E. Malvern, Introduction to the Mechanics of a Continuous Medium, Prentice Hall, Englewood Cliffs (N.J.), 1969.
[33] J. Gough, I.H. Gregory, A.H. Muhr, Determination of Constitutive Equations for Vulcanized Rubber, in: D. Boast, V.A. Coveney (Eds.), Finite Element Analysis of Elastomers, Professional Engineering Publishing, Bury St Edmunds, 1999, pp. 5–26.
[34] E.N. Dvorkin, M.B. Goldschmit, Nonlinear Continua, Springer–Verlag, Berlin, 2006.
[35] R.S. Rivlin, Large Elastic Deformations of Isotropic Materials. IV. Further Developments of the General Theory, Philosophical Transaction of the Royal Society of London. Series A, Mathematical and Physical Sciences, 241 (1948) 379–397.
[36] O.H. Yeoh, Some forms of the strain-energy function for rubber, Rubber Chemistry and Technology, 66 (1993) 754–771.
[37] E.M. Arruda, M.C. Boyce, A Three–Dimensional Constitutive Model for the Large Stretch Behavior of Rubber Elastic Materials, Journal of the Mechanics and Physics of Solids, 41 (1993) 389–412.
[38] R.S. Marlow, A general first-invariant hyperelastic constitutive model, in: J.J.C. Busfield, A.H. Muhr (Eds.), Constitutive Models for Rubber III, Taylor & Francis, 2003, pp. 157–160.
[39] J.R. Daley, S. Mays, The Complexity of Material Modelling in the Design Optimization of Elastomeric Seals, in: D. Boast, V.A. Coveney (Eds.), Finite Element Analysis of Elastomers, Professional Engineering Publishing, Bury St Edmunds, 1999, pp. 119–128.
[40] D. Cadge, A. Prior, Finite Element Modelling of Three-Dimensional Elastomeric Components, in: D. Boast, V.A. Coveney (Eds.), Finite Element Analysis of Elastomers, Professional Engineering Publishing, Bury St Edmunds, 1999, pp. 187–205.

[41] K.J. Bathe, Finite Element Procedures, Prentice Hall, Upper Saddle River (N.J.), 1996.
[42] R. Johannknecht, S. Jerrams, G. Clauss, The Uncertainty of Implemented Curve-Fitting Procedures in Finite Element Software, in: D. Boast, V.A. Coveney (Eds.), Finite Element Analysis of Elastomers, Professional Engineering Publishing, Bury St Edmunds, 1999, pp. 141–151.
[43] E.H. Twizell, R.W. Ogden, Non-linear optimization of the material constants in Ogden's stress-deformation function for incompressible isotropic elastic materials, Journal of Australian Mathematical Society, Series B, 24 (1983) 424–434.
[44] A. Bucchi, G.E. Hearn, Predictions of Aneurysm Formation in Distensible Tubes – Part B – Application and Comparison of Alternative Approaches, International Journal of Mechanical Sciences, XX (2013) YYY–YYY.
[45] J. Turner, D. Boast, R. Jarosz, Definitions and Calculations of Stress and Strain in Rubber, in: D. Boast, V.A. Coveney (Eds.), Finite Element Analysis of Elastomers, Professional Engineering Publishing, Bury St Edmunds, 1999, pp. 61–74.
[46] ABAQUS®, Theory Manual (v. 6.9) (2009).
[47] L.R.G. Treloar, The Physics of Rubber Elasticity, Clarendon Press, Oxford, 1949
[48] H. Alexander, A constitutive relation for rubber-like materials, International Journal of Engineering Science, 6 (1968) 549–563.
[49] K.J. Bathe, G.A. Ledezma, Benchmark problems for incompressible fluid flows with structural interactions, Computers and Structures, 85 (2007) 628–644.
[50] W.B. Shangguan, Z.H. Lu, Modelling of a hydraulic engine mount with fluid-structure interaction finite element analysis, Journal of Sound and Vibration, 275 (2004) 193–221.
[51] M.L. Raghavan, D.A. Vorp, Toward a biomechanical tool to evaluate rupture potential of abdominal aortic aneurysm: identification of a finite strain constitutive model and evaluation of its applicability, Journal of Biomechanics, 33 (2000) 475–482.
[52] C. Lally, A.J. Reid, P.J. Prendergast, Elastic Behavior of Porcine Coronary Artery Tissue under Uniaxial and Equibiaxial Tension, Annals of Biomedical Engineering, 32 (2004) 1355–1364.
[53] Y. Papaharilaou, J.A. Ekaterinaris, E. Manousaki, A.N. Katsamouris, A decoupled fluid structure approach for estimating wall stress in abdominal aortic aneurysm, Journal of Biomechanics, 40 (2007) 367–377.
[54] B.J. Doyle, J. Killion, A. Callanan, Use of the photoelastic method and finite element analysis in the assessment of wall strain in abdominal aortic aneurysm models, Journal of Biomechanics, 45 (2012) 1759–1768.
[55] L.J. Hart-Smith, Elasticity Parameters for Finite Deformations of Rubber-Like Materials, Zeitschrift für Angewandte Mathematik und Physik (ZAMP), 17 (1966) 608–626.

[56] K.C. Valanis, R.F. Landel, The Strain−Energy Function of a Hyperelastic Material in Terms of the Extension Ratios, Journal of Applied Physics, 38 (1967) 2997–3002.
[57] D.F. Jones, L.R.G. Treloar, The properties of rubber in pure homogeneous strain, Journal of Physics D: Applied Physics, 8 (1975) 1285–1304.
[58] L.R.G. Treloar, The elasticity of a network of long-chain molecules. I., Transactions of the Faraday Society, 39 (1943) 36–41.
[59] W. Kuhn, Dependence of the average transversal on the longitudinal dimensions of statistical coils formed by chain molecules, Journal of Polymer Science, 1 (1946) 380–388.
[60] J.M. Gere, B.J. Goodno, Mechanics of Materials, seventh ed., Cengage Learning, Stamford, 2008.
[61] S.P. Timoshenko, History of Strength of Materials, Dover Publications, Mineola (N.Y.), 1983.
[62] J.D. Humphrey, Computer Methods in Membrane Biomechanics, Computer Methods in Biomechanics and Biomedical Engineering, 1 (1998) 171–210.
[63] A.E. Green, J.E. Adkins, Large Elastic Deformations and Non-linear Continuum Mechanics, Clarendon Press, Oxford, 1960.
[64] J.R. Dormand, P.J. Prince, A family of embedded Runge-Kutta formulae, Journal of Computational and Applied Mathematics, 6 (1980) 19–26.
[65] L.R. Herrmann, Elasticity Equations for Incompressible and Nearly Incompressible Materials by a Variational Theorem, AIAA Journal, 3 (1965) 1896–1900.
[66] E.P. Kasper, R.L. Taylor, A mixed-enhanced strain method Part I: Geometrically linear problems, Computers & Structures, 75 (2000) 237–250.
[67] E.P. Kasper, R.L. Taylor, A mixed-enhanced strain method Part II: Geometrically nonlinear problems, Computers & Structures, 75 (2000) 251–260.
[68] J.N. Reddy, An Introduction to Nonlinear Finite Element Analysis, Oxford University Press, New York, 2004.
[69] D. Pantuso, K.J. Bathe, On the stability of mixed finite elements in large strain analysis of incompressible solids, Finite Elements in Analysis and Design, 28 (1997) 83–104.
[70] A. Ramsay, Recent Developments in Finite Element Analysis of Elastomeric Components, in: D. Boast, V.A. Coveney (Eds.), Finite Element Analysis of Elastomers, Professional Engineering Publishing, Bury St Edmunds, 1999, pp. 223–232.
[71] E.N. Dvorkin, On the convergence of incompressible finite element formulations. The Patch Test and the inf-sup condition, Engineering Computations, 18 (2001) 539–556.
[72] T.J.R. Hughes, The finite element method: Linear Static and Dynamic Finite Element Analysis, Prentice Hall, 1987.

[73] A. Prior, D. Cadge, Finite Element Analysis of Contact and Hyperelastic Materials, in: D. Boast, V.A. Coveney (Eds.), Finite Element Analysis of Elastomers, Professional Engineering Publishing, Bury St Edmunds, 1999, pp. 129–140.
[74] R.G. Toscano, E.N. Dvorkin, A shell element for finite strain analyses: hyperelastic material models, International Journal for Computer-Aided Engineering and Software, 24 (2007) 514–535.
[75] B.J. Doyle, A. Callanan, P.E. Burke, P.A. Grace, M.T. Walsh, D.A. Vorp, T.M. McGloughlin, Vessel asymmetry as an additional diagnostic tool in the assessment of abdominal aortic aneurysms, Journal of Vascular Surgery, 49 (2) (2009) 443–454.
[76] T.C. Gasser, M. Auer, F. Labruto, J. Swedenborg, J. Roy, Biomechanical Rupture Risk Assessment of Abdominal Aortic Aneurysms: Model Complexity versus Predictability of Finite Element Simulations, European Journal of Vascular & Endovascular Surgery, 40 (2010) 176–185.
[77] A. Maier, M.W. Gee, C. Reeps, J. Pongratz, H.H. Eckstein, W.A. Wall, A Comparison of Diameter, Wall Stress, and Rupture Potential Index for Abdominal Aortic Aneurysm Rupture Risk Prediction , Annals of Biomedical Engineering, 38 (2010) 3124–3134.
[78] O.C. Zienkiewicz, R.L. Taylor, The Finite Element Method, Vol. I: The Basis, fifth ed., Butterworth-Heinemann, Oxford, 2000.
[79] K.J. Bathe, E. Ramm, E.L. Wilson, Finite element formulation for large deformation dynamic analysis, International Journal for Numerical Methods in Engineering, 9 (1975) 353–386.
[80] T. Sussman, K.J. Bathe, A finite element formulation for nonlinear incompressible elastic and inelastic analysis, Computers & Structures, 26 (1987) 357–409.
[81] J.N. Reddy, An Introduction to Continuum Mechanics with Applications, Cambridge University Press, Cambridge, 2008.
[82] G.A. Holzapfel, Nonlinear solid mechanics: a continuum approach for engineering, John Wiley & Sons, Chichester, 2000.
[83] K.J. Bathe, The inf–sup condition and its evaluation for mixed finite element methods, Computers & Structures, 79 (2001) 243–252.
[84] F. Brezzi, M. Fortin, Mixed and Hybrid Finite Element Methods, Springer–Verlag, New York, 1991.
[85] ABAQUS®, User's Manual Volume IV: Elements (v. 6.9) (2009).
[86] F. Auricchio, M. Di Loreto, E. Sacco, Finite-element Analysis of a Stenotic Artery Revascularization through a Stent Insertion, Computer Methods in Biomechanics and Biomedical Engineering, 4 (2001) 249–263.

[87] V. Prot, B. Skallerud, G. Sommer, G.A. Holzapfel, On modelling and analysis of healthy and pathological human mitral valves: Two case studies, Journal of the Mechanical Behavior of Biomedical Materials, 3 (2010), 167–177.
[88] J.F. Rodriguez, C. Ruiz, M. Doblaré, G.A. Holzapfel, Mechanical Stresses in Abdominal Aortic Aneurysms: Influence of Diameter, Asymmetry, and Material Anisotropy, Journal of Biomechanical Engineering, 130 (2008) 021023–1 – 021023–10.
[89] F. Migliavacca, L. Petrini, M. Colombo, F. Auricchio, R. Pietrabissa, Mechanical behaviour of coronary stents investigated through the finite element method, Journal of Biomechanics, 35 (2002) 803–811.
[90] Y.P. Korkolis, S. Kyriakides, Hydroforming of anisotropic aluminium tubes: Part II analysis, International Journal of Mechanical Sciences, 53 (2011) 83–90.
[91] ABAQUS®, Verification Manual (v. 6.9) (2009).
[92] K.Y. Sze, X.H. Liu, S.H. Lo, Popular benchmark problems for geometric nonlinear analysis of shells, Finite Elements in Analysis and Design, 40 (2004) 1551–1569.
[93] D.S. Malkus, T.J.R. Hughes, Mixed Finite Element Methods – Reduced and Selective Integration Techniques: a Unification of Concepts, Computer Methods in Applied Mechanics and Engineering, 15 (1978) 63–81.
[94] M.S. Gadala, Alternative Methods for the Solution of Hyperelastic Problems with Incompressibility, Computers & Structures, 42 (1992) 1–10.
[95] P. Wriggers, Nonlinear Finite Element Methods, Springer–Verlag, Berlin, 2008.
[96] M.A. Crisfield, Non-linear Finite Element Analysis of Solids and Structures. Volume 2: Advanced Topics, John Wiley & Sons, Chichester, 1997.
[97] S.A. Ragon, Z. Gurdal, L.T. Watson, A comparison of three algorithms for tracing nonlinear equilibrium paths of structural systems, International Journal of Solids and Structures, 39 (2002) 689–698.
[98] J. Shi, Computing Critical Points and Secondary Paths in Nonlinear Structural Stability Analysis by Finite Element Method, Computers & Structures, 58 (1996) 203–220.
[99] B.Z. Huang, S.N. Atluri, A Simple Method to Follow Post-Buckling Paths in Finite Element Analysis, Computers & Structures, 57 (1995) 477–489.
[100] R.T. Shield, On the Stability of Finitely Deformed Elastic Membranes – Part I Stability of a Uniformly Deformed Plane Membrane, Zeitschrift für Angewandte Mathematik und Physik (ZAMP), 22 (1971) 1016–1028.

[101] R.T. Shield, On the Stability of Finitely Deformed Elastic Membranes – Part II Stability of Inflated Cylindrical and Spherical Membranes, Journal of Applied Mathematics and Physics (ZAMP), 23 (1972) 16–34.
[102] B.D. Reddy, A Deformation-Theory Analysis of the Bifurcation of Pressurised Thick-Walled Cylinders, The Quarterly Journal of Mechanics and Applied Mathematics, 35 (1982) 183–196.
[103] D.M. Haughton, R.W. Ogden, Bifurcation of Inflated Circular Cylinders of Elastic Material Under Axial Loading – I. Membrane Theory for Thin-Walled Tubes, Journal of the Mechanics and Physics of Solids, 27 (1979) 179–212.